University of Stavanger

FACULTY OF SCIENCE AND TECHNOLOGY

MASTER'S THESIS

Study programme/specialisation: Natural Gas Technology	Spring/ Autumn semester, 20.20. Open / Confidential
Author: Joan Shanita Wanyenze	
Programme coordinator: Supervisor(s): A.H. Rabenjafimanantsoa, Hans Joakim Skadsem & Rune Wiggo Time	
Title of master's thesis: Small scale thermohaline ocean circulation	
Credits: 30 pts	
Keywords: - Thermohaline circulation - Stommel model - Ocean circulation - Overturn circulation - Freshwater input	Number of pages: 56 (excl. front page) + supplemental material/other: ……-…… Stavanger, ……15/07-20…….. date/year

Acknowledgments

The following experiment was conducted at the University of Stavanger (UiS) at the Mesanin laboratory over the course of 6 months. I would like to acknowledge my supervisors A.H. Rabenjafimanantsoa, Hans Joakim Skadsem and Rune Wiggo Time with their expertise and guidance throughout the duration of this thesis work, which pushed me beyond my limits and made me to think creatively. Furthermore, my fellow laboratory students, who in times of distress and hardships stood together collectively with moral support. And last but not least, my dear family for showing me that focus is paramount in everything.

To God be the Glory.

Joan Shanita Wanyenze

Abstract

Upon examining the how convective flows are generated in the ocean, Henry Stommel presented a simple idealized model called the Stommel model (1961) to better understand how salinity and temperature differences can affect the ocean circulation between the Arctic and Atlantic. The ocean circulation is named thermohaline circulation. This thesis implements the Stommel model using a small scale setup filled with a salt mixture including external systems duplicating the Arctic and Atlantic like the buffer system and evaporation system respectively. A mass balance of the salt content is to preserved throughout the experiment, however it was observed that this was not the case. Despite some mishaps in the data collection, measurements of the conductivity show lessened value in both basins plus a salt accumulation in the evaporation system meaning an ineffective salt drive to the Atlantic basin. It was also observed that the freshwater input reached a maximum limit and transitions between the circulation modes were abrupt. Suggestions to modifications in terms of the setup were discussed, however these have some limitations. Nonetheless, this thesis can be used a precursor to see how complex and diverse the thermohaline circulation really is.

Table of Contents

Nomenclature . . . . . **v**

List of Tables . . . . . **vi**

List of Figures . . . . . **vii**

1 Introduction **1**

2 Theory **4**

2.1 Thermohaline circulation 4

2.2 Stommel's two box model 5

3 Experimental Setup **11**

3.1 The small scale rig setup 11

3.2 Rig elements and systems 12

3.2.1 Circulation system 12

3.2.2 Temperature regulation system 13

3.2.3 Evaporation system 13

3.2.4 Salinity regulation system 14

3.3 Measurement and control systems 17

4 Results and discussions **19**

5 Conclusions **27**

References **29**

Matlab code **30**

A Procedures **36**

B Additional equations **41**

C Additional figures **45**

Nomenclature

Abbreviations:

THC	Thermohaline circulation	
AMOC	Atlantic Meridional Ocean Circulation	
RPM	Rotations per minute	
PVC	Polyvinyl chloride	
OD	Outer diameter	m
ID	Inner diameter	m

Roman and greek letters:

T	Temperature	°C
S	Salinity	mS/cm
W	Power	$kg \cdot m^2 \cdot s^{-3}$
Sv	Sverdrup	$10^6 m^3/s$
ρ	Density	kg/m^3
c	Temperature transfer coefficient	s^{-1}
d	Salinity transfer coefficient	s^{-1}

List of Tables

2.1 Solutions on equilibrium points by variation in parameters. 8
3.1 Pipe dimensions for small scale setup. "w" stands for width and "h" stands for height. 11
4.1 Mettler Toledo readings of the calibration solution after averaging. 22
A.1 Conductivity standard values for manufactured Mettler Toledo solutions. 37

List of Figures

1.1 The five commonly known ocean gyres on Earth. The direction of the circulations is different between the Northern- and Southern Hemisphere (Motion, n.d.). 2
2.1 An illustration of the ocean circulation known as the THC. (Research Center, n.d.) 4
2.2 Upper overflow is included so that surface level in both basins is maintained. A positive flow q from basin 1 to basin 2, where the porous walls permit exchange in heat and salt internally for each basin. (Walsh, 2019) 6
2.3 A loss of freshwater influx F contributes to a zero salinity change thus implying an end to a haline circulation. 9
2.4 A zero salinity change generates equal salinity in both basins thus giving way to a thermal regime. Blue stands for basin 2 (Arctic) and red for basin 1 (Atlantic). . . 10
2.5 An increase in pipe and Arctic temperature generates a lower overturn. The red dots apply to the case of a $4m$ pipe height indicating a return to a stable thermal regime. 10
3.1 A detailed illustration of the preexisting small scale setup. 12
3.2 Valves and couplings used in the small scale setup. 12
3.3 An illustration of the thermo regulation system. Notice how the direction of both flows is opposite to each other. 14
3.4 An illustration of the evaporation system. 15
3.5 An illustration of buffer system included in the salt regulation system. Notice how the two tanks are at different levels. This is ensure flow through the capillary pipe due to gravity difference. 17
3.6 An illustration of the lower flow meter. 18
3.7 An illustration of the upper flow meter. 18
3.8 An illustration of the external measurement and control systems.. The Erlenmeyer flasks are replaced as shown in fig. C.1 on page 45. An explanation as to why is found in section 4.2 under chapter 4. 19
4.1 First run after calibration before changing Arctic basin temperature with the upper valve closed. 20
4.2 Third run after proper calibration, replacing defect A4 sensor and lowering Arctic water bath temperature. 21

4.3 Mettler Toledo values of calibration solution after averaging. An increase in the R^2-number compared to figure C.7 on page 48. 21
4.4 Logarithmic scale of the voltage and intensity from the regulator and power meter respectively. 22
4.5 The behaviour of temperature sensors during the experiment proved to show how sensitive they are. Notice how $P1$ has the most disturbances, which can be due to the massive down flow passing the sensor as it is situated near the upper flow meter. 23
4.6 The flow of the freshwater input in the upper flow meter. The peaks prior to the start of the experiment are due to pressing of capillary tubes at the flow meter. The y-axis is shortened for detail. 24
4.7 Overturn flow in the lower flow meter. There is no indication of any flow through the flow meter even after thorough inspection of the system insuring no blocked passages. 25
4.8 The conductivity in both basins follow each other. From the figure, we see that 40 min after start, the conductivity in both basins drops. 26
5.1 A simplified model of the THC simulated in STELLA© software primarily used to study abrupt climate change. 27
A.1 An illustration of the power supply to the evaporation system. 40
B.1 Heat and salinity are exchanges between the compartments through the porous walls with constant temperature T* and salinity S*. (Walsh, 2019) 41
B.2 Inflow and outflow is included with incoming water at a fixed temperature $T = T_{in}$ and salinity $S = S_{in}$. (Walsh, 2019) 43
C.1 The Erlenmeyer flasks shown in figure fig. 3.8 on page 19 are replaced with a three way passage connector, with a small capillary tube connected to the top passage with a clamp to ensure a constant pressure while pumping. 45
C.2 The replacement valve installed by the evaporation system in fig. 3.4 on page 15 and the Atlantic basin water bath. The flow meter was used to ensure that the water level in the evaporation system was constant. 45
C.3 First run before calibration. A lot of oscillations. 46
C.4 Second run before calibration. No different from figure C.3. 46
C.5 Third run before calibration. Starting point for few sensors is lowered. 47
C.6 Second run after calibration and lowered Arctic water bath temperature with defect A4 sensor. 47
C.7 Mettler Toledo values of the calibration solution before averaging with formula and R^2-number. 48
C.8 Sensors $P4$ and $A4$ are both inserted with a plastic pipe. 48

1 Introduction

The quest to understand more about the depths of the ocean and waters at large dates back to primordial times. It started with acquiring provision by ocean diving in 4000 BC, exploring new territories starting from the 15th century and continues on with present-day technological inventions. There are 5 major ocean basins on Earth: Atlantic, Pacific, Indian, Southern and Arctic. The oceans cover 71 percent of the Earth's surface and contains 97 percent of the Earth's water (Hawaii Pacific University, n.d.). Intuitively, ocean waters are always in motion. Even at very low wind currents, there is movement occurring on the surface water. Waves and tides are defined as transfer of energy through advection, which is energy transfer through a flow of a fluid. However, ocean circulation is not only driven by waves and tides due to gravity of the moon and sun, but also from density differences. There are 3 main layers of the ocean waters: the surface layer, deep ocean and seafloor sediment. The transition zone between the first two layers is called the **thermocline**, which can change at different latitudes and seasons (Stommel, 1961). The surface currents are generally driven by wind currents moving in the same direction with an offset in angle by the Coriolis effect (Webb, 2019). Due to this effect, low latitude equatorial currents at $0 - 30°$ will be deflected to the Northern- and Southern Hemisphere, thus delivering warm currents to the middle and higher latitudes of $30 - 90°$ (Webb, 2019). At the same time, the high latitude areas of $60 - 90°$ deliver cold surface currents to lower latitude areas (Webb, 2019). All this combined creates a conglomerate of surface circulation currents named ocean gyres. The direction of the gyres is shown in fig. 1.1 on the next page. In the Northern Hemisphere, the circulation is clockwise, while it is the opposite for the Southern Hemisphere.

As nature has it, the ocean currents flow for great distances thus creating paths called global conveyor belts and are measured in the non-SI unit **sverdrup** (sv), where $1sv$ is equivalent to volume flow rate of $1 \cdot 10^6 m^3/s$. These conveyor belts determine the temperature and salinity of the region in which they voyage through. An example of a surface current conveyor belt is the Gulf Stream. The convergence of the North Atlantic Equatorial currents and the Florida current create this stream as shown in fig. 1.1 on the following page. Both currents bring warm ocean waters along the eastern coastal line of the U.S continent and extends all the way to the Northern Sea. The Gulf Stream is crucial to the global climate as it provides moderating temperatures in areas such as the coast of Florida with warm temperatures and Western Europe with mild temperatures during the winter (Encyclopedia, n.d.). The movement of surface currents happen in two distinctive patterns which work coherently. Upwelling, in simple terms, brings mineral rich cold deep water to the mineral deprived surface currents. Amongst the many examples are Humboldt current (coast of Peru) and the Somali current (between Somali and Oman). Downwelling, on the other hand, occurs when surface currents converge, thus pushing them down. Therefore mineral deprived surface

currents are pushed down and consequently creating ocean zones with low biological productivity contrary in the case of upwelling. An example is the Labrador coast in Canada. Since surface

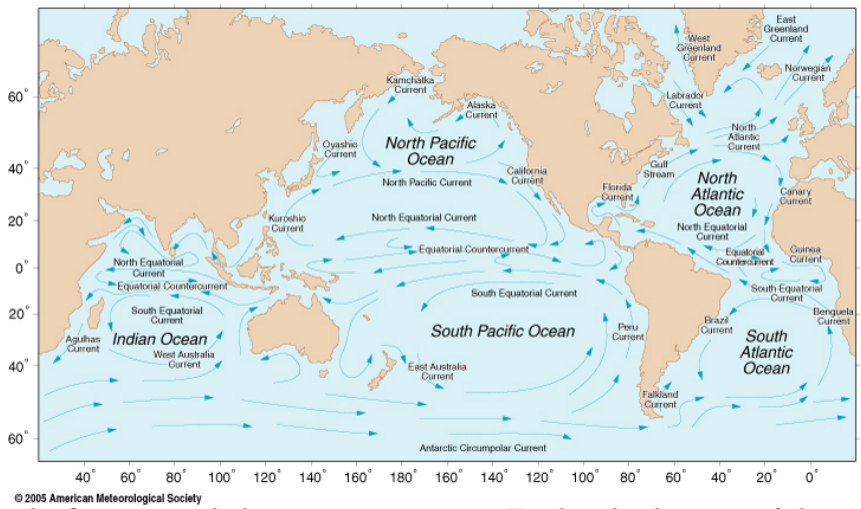

Figure 1.1: The five commonly known ocean gyres on Earth. The direction of the circulations is different between the Northern- and Southern Hemisphere (Motion, n.d.).

currents only involve surface water and are driven by wind, only 10 percent of the ocean's volume is affected by them. This means that the remaining 90 percent involve water movements. In other words, the currents are driven by water density differences. This phenomenon takes place in the second layer of the ocean called the deep waters. Less dense ocean water (warm) overlays more dense waters (cold) thus creating an ocean circulation. Besides from this, given the contrasting behaviour between upwelling and downwelling, zones with heterogeneous salinity and temperature values are generated throughout the global ocean. The NORTH project is an initiative by the Bjerknes Climate Centre used to examine the convective flows in the ocean especially between the Arctic and Atlantic ocean. The convective flow of interest is the thermohaline circulation, where *thermo* defines T and *haline* defines S. The project does not only consider the core fundamentals, but also how climate change and external feedback such as freshwater input can affect the THC.

The purpose of this thesis is to emulate the THC in a small scale model while applying the Stommel model (1961). The analysis and study in this thesis is purely experimental and uses the NORTH project as a precursor. A medium scale model was planned for comparison, however this was not executed due to unforeseeable circumstances. In chapter 2, a thorough description of the THC is presented with complimentary theory about the Stommel mode. A MATLAB code by Professor Rune Time Wiggo is simulated to show how change in physical parameters can affect properties of the THC. Additional theory is found in Appendix B. Furthermore, chapter 3 shows how details the setup with a descriptive outline of internal and external systems used during the experiment. Moreover, chapter 4 presents the results retrieved from collected data with discussions included alongside and an outline of procedures in Appendix A. Any suggestions to better the work is also

included in this chapter. And in closing, chapter 5 presents the conclusions about the experiment.

2 Theory

2.1 Thermohaline circulation

While currents and tides are driven by wind due to the gravity of the moon and sun, the *thermohaline circulation* (THC), on the other hand, is driven by density differences in seawater as shown in fig. 2.1. In other words by exchanges of heat and freshwater input on the sea surface and the mixing of heat and salt (Rahmstorf, 2006). Seawater density is conditioned by three properties: temperature, salinity and pressure. Temperature has the greatest impact on seawater density. A decrease in temperature with increasing depth indicates in an increase in density. A decrease in salinity, on the other hand, indicates a decrease in density. The contrasting results from temperature and salinity is due to their coefficients respectively. The thermal expansion α is considered a negative value, whereas the contraction coefficient β is of positive value. Lastly, pressure has the least effect on seawater density as water is considered incompressible under normal conditions, however it is of significance at extremely high depths (Webb, 2019, p. 135).

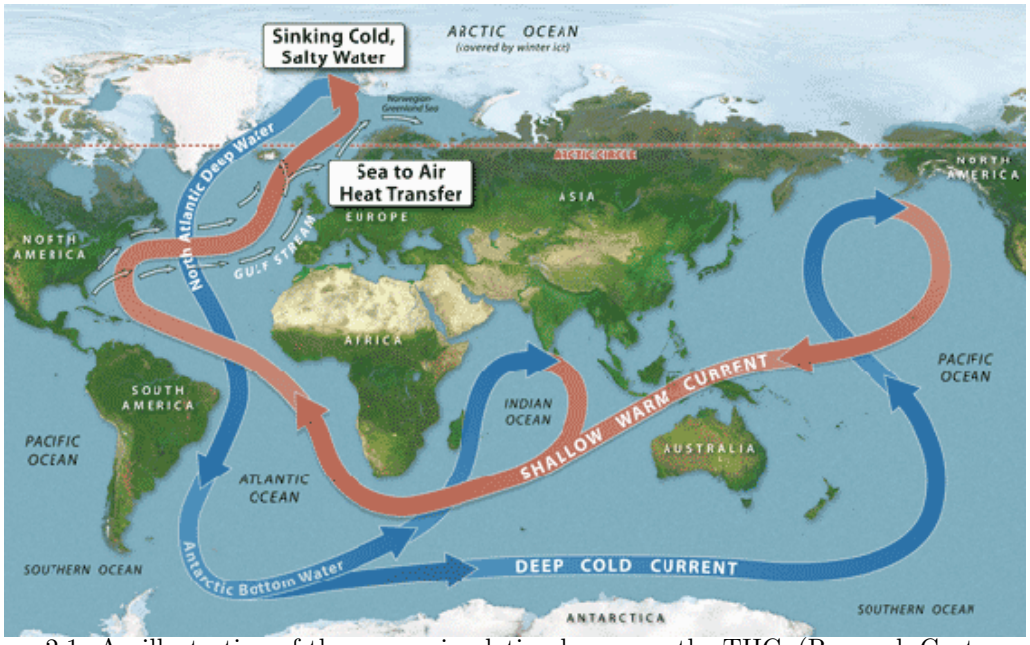

Figure 2.1: An illustration of the ocean circulation known as the THC. (Research Center, n.d.)

Idealized box models used to describe density-driven circulation and two layer flow dates back in 1687 by Italian scholar Luigi Ferdinando Marsili. The commonly known box model is by Henry Stommel (1961). A 2-box model with a cool basin and a warm basin, representing the Arctic and Atlantic ocean respectively, with well mixed water masses. Although the box model was not explicitly applied to the ocean by Stommel, it clearly illustrates how Atlantic waters are subject to net evaporation, while Arctic waters are subject to precipitation. The latter is filled with cold dense water from surface to bottom at high latitudes, while the former with an upper layer of

warm and light water at low latitudes. A freshwater influx is included in the box model. Stommel showed that a significant influx of freshwater can reverse THC and deem it salinity-dominated. Therefore, Stommel concluded that the box model can maintain density-driven circulation either by temperature or salinity. On the other hand, a second theory suggests mechanical energy is needed to drive THC. This can be achieved by a deep water mixing (Munk and Wunsch, 1998). Freshly formed deep water is product of deep mixing transformation of cold dense water into warm water[1]. A third theory suggests that upwelling with mixing in the upper layer contributes a lot to THC[2]. One would wonder then which of the theories is valid and it depends on the time scale (Rahmstorf, n.d.; Robinson and Stommel, 1959). In the long run, the last two theories will apply to THC, however, in shorter time scales, density differences will characterize THC.

This begs to show that the Stommel model does not take into account water mass transformations governed by mixing and surface buoyancy forcing. An earlier publication conducted by Stommel and Rooth (1968) examined the impact of wind stress on THC. Further publications such as Guan and Huang (2008) and Oka, Hasumi, and Suginohara (2001) detail the impact of wind stress with more complex models. In order to include the water mass transformations, a framework was suggested by Walin (1977; 1982) using temperature- and salinity coordinates rather than vertical or horizontal ocean currents. In other words, the relationship between the three theories can be explained using a temperature-salinity scope. This framework has been the basis of further studies on how freshwater input can impact THC. Studies such as Rennermalm et al. (2006), Lambert, Eldevik, and Haugan (2016) and Otterå and Drange (2004) examine the sensitivity and stabilisation of THC to freshwater input in the Arctic basin.

2.2 Stommel's two box model

As mentioned in the previous section, Stommel (1961) suggested a simple idealized model designed to comprehend the ocean circulation between the Arctic and Atlantic basin. The box models presented in Appendix B.1 and B.2 on page 41 to 43 are a basis for the 2-box idealized model in fig. 2.2 on the following page. Therefore they are not applicable to natural conditions, however, they are considered preliminaries for explaining how flow rates in convective systems depend upon density differences (Stommel, 1961, p.226). We consider two well-mixed basins connected with a capillary tube at the bottom with an overflow at the top so as to maintain the volume in both basins ((Walsh, 2019)). Each basins has outer vessels with constant temperature T_i^* and salinity

[1] Munk and Wunsch concluded that external forces, such as wind stress and tidal dissipation, contribute to the mechanical energy. This is in contrast the buoyancy flux theorem explaining the density-driven circulation THC. For that same reason, Munk and Wunsh preferred to use the term meridional overturning circulation.

[2] This theory is a basis of Toggweiler and Samuel (1993). Upwelling is wind-driven motion of cold dense water up to the ocean surface replacing warm surface water. With upwelling occuring in the Southern Ocean, NADW is pulled up to the surface suggesting a strong Ekman upwelling around 50-60° latitudes.

S_i^*, where $i = 1$ is warm basin and $i = 2$ is cold basin.

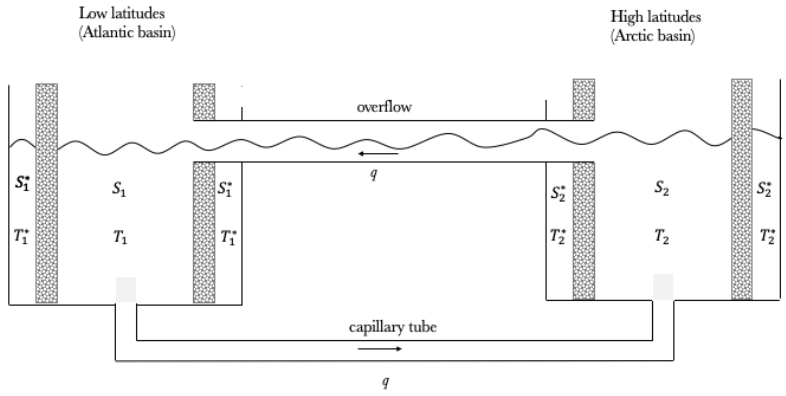

Figure 2.2: Upper overflow is included so that surface level in both basins is maintained. A positive flow q from basin 1 to basin 2, where the porous walls permit exchange in heat and salt internally for each basin. (Walsh, 2019)

The box model above is to be examined as a whole, thus by defining a single temperature $T = T_1 = -T_2$ and salinity $S = S_1 = -S_2$[3], change in the properties over time can be determined by differentiation. Given that a capillary flow q is present, this is also included as a constant $|2q|$ and c, d are dimensionless constants (Walsh, 2019).

$$\frac{dT}{dt} = c(T^* - T) - |2q|T \tag{2.2.1}$$

$$\frac{dS}{dt} = d(S^* - S) - |2q|S \tag{2.2.2}$$

On the quest to further simplify the equations above, we nondimensionalize all physical properties by substitution of variables. The physical properties examined at first are T, S and T^*, S^*. Since we have defined a single temperature T and salinity S, it is also evident to do the same for the fixed values T_i and S_i by defining $T^*_{ave} = \frac{1}{2}(T_1^* + T_2^*)$ and $S^*_{ave} = \frac{1}{2}(S_1^* + S_2^*)$. Thus by setting $u_i = T_i - T^*_{ave}$ and $v_i = S_i - S^*_{ave}$ we get the equations below (Walsh, 2019).

$$\frac{du}{dt} = c(u^* - u) - |2q|u \tag{2.2.3}$$

$$\frac{dv}{dt} = d(v^* - v) - |2q|v \tag{2.2.4}$$

The above equation has one physical property left, q, thus by setting $x = v/v^*$, $y = u/u^*$, $\tau = ct$ dimensionless time, $\delta = d/c$ dimensionless ratio between the salinity transfer and temperature

[3]Stommel came to this conclusion by assuming symmetry in the box model given that the surface level in each basin remains the same provided an upper overflow as shown in fig. 2.2.

transfer coefficient, and $f = 2q/c$ a dimensionless flow rate, we get as follows below. (Walsh, 2019)

$$\begin{aligned}
\frac{du}{dt} &= c(u^* - u) - |2q|u \\
\frac{d(yu^*)}{d(\tau/c)} &= c(u^* - u) - |2q|u \\
\frac{dyu^* + ydu^*}{(d\tau c - \tau dc)/c^2} &= c(u^* - u) - |2q|u \\
u^* \frac{c^2 dy}{d\tau c} &= c(u^* - u) - |2q|u \\
u^* \frac{dy}{d\tau} &= (u^* - u) - |f|u \\
\frac{dy}{d\tau} &= 1 - y - |f|y
\end{aligned} \tag{2.2.5}$$

$$\begin{aligned}
\frac{dv}{dt} &= d(v^* - v) - |2q|v \\
\frac{d(xv^*)}{d(\tau/c)} &= d(v^* - v) - |2q|v \\
\frac{dxv^* + xdv^*}{(d\tau c - \tau dc)/c^2} &= d(v^* - v) - |2q|v \\
v^* \frac{c^2 dx}{d\tau c} &= d(v^* - v) - |2q|v \\
v^* \frac{xy}{d\tau} &= \sigma(v^* - v) - |f|v \\
\frac{dx}{d\tau} &= \sigma(1 - x) - |f|x
\end{aligned} \tag{2.2.6}$$

While equations 2.2.5 and 2.2.6 are designed to their properties respectively, including a ratio parameter of these properties into the mentioned equations could further show how they vary over time. Inserting $\lambda f = -y + Rx$, where $\lambda = kc/4\rho_0\alpha u^*$ and $R = \beta v^*/\alpha u^*$ a measure of ratio of effect of salinity and temperature on the density (Stommel, 1961; Walsh, 2019) into the above equations gives equations 2.2.7 and 2.2.9, where the latter is an equilibrium solution (Walsh, 2019). Thus eliminating f shows that the dimensionless properties x and y (salinity and temperature respectively) depend on the coefficients β and α for salinity and temperature respectively. Furthermore, the flow q can also be expressed in terms of the ratio R as shown in equation (2.2.8), where λ is a dimensionless flow resistance. (Walsh, 2019)

$$\begin{aligned}
\frac{dx}{d\tau} &= \sigma(1 - x) - \frac{1}{\lambda}|y - Rx|x \\
\frac{dy}{d\tau} &= 1 - y - \frac{1}{\lambda}|y - Rx|y
\end{aligned} \tag{2.2.7}$$

$$kq = 2\rho_0\alpha u^*(-y + Rx) \tag{2.2.8}$$

An increase in temperature differences between basins implies that $\alpha >$ salinity coefficient β, in other words $R < 1$. Therefore the state of evaporation will govern the density differences with

cold dense waters from basin 2 emigrating towards less dense waters in basin 1. Hence the flow q will be the opposite of that depicted in fig. 2.2 on page 6. On the other hand, if $\alpha < \beta$, then precipitation creates a deep water flow from saltier basin 1 to less salty basin 2 implying that $q > 0$. (Walsh, 2019)

$$\begin{aligned} \lambda f &= -y^* + Rx^* \\ &= -\frac{1}{1+|f|} + \frac{R\sigma}{\sigma+|f|} \equiv \phi(f, R, \sigma) \end{aligned} \tag{2.2.9}$$

By equating eq. (2.2.9) to 0, three equilibria points are generated from under the conditions that $R\delta < 1$ if $R > 1$ or $R\delta > 1$ if $0 < R < 1$ (Stommel, 1961). Recalling that R is a measure of ratio of effect of salinity and temperature on the density differences, at first hand, the first condition would imply a stable node where a haline regime will dominate the flow q. The second condition is limited by a range, consequently, it would generate the remaining equilibria points named stable spiral and saddle point, where the latter is deemed unstable. And given that $0 < R < 1$, the second condition will generate an unstable and stable thermal regime in regards to the flow q. The determination of the final circulation regime not only depends on R, but also on variations in the parameters δ and λ. Table 2.1 below shows how a variation in the parameters determines the final circulation mode[4]. (Stommel, 1961)

Table 2.1: Solutions on equilibrium points by variation in parameters.

System	$R = 2$	$\delta = \frac{1}{6}$	$\lambda = \frac{1}{5}$	$R = 2, \delta = 1, \lambda = \frac{1}{6}$
f	-1.10	-0.30	+0.23	+1.76
Case	$y > Rx$	$y > Rx$	$y < Rx$	$y < Rx$
Equilibrium point	Stable node	Saddle point	Stable spiral	Stable node

An intriguing point of view is whether transitions between the circulation modes are abrupt given that a slight increase in λ does produce contrasting results (Walsh, 2019). And if so, whether an external agent can contribute to a stabilised circulation mode in the long run in the box model. Given that Stommel did not consider climate change into his conceptual model, this did not hinder future publications such as Lohmann and Gerdes (1998), Whitehead (2009) and Cheng et al. (2018) to address how freshwater influxes due to sea ice melt and river runoffs can affect THC. Freshwater influxes intermix with saline water and are often expressed in terms of mSv due to its marginal scale compared to oceanic volume transports expressed in Sv. The freshwater flux F is expressed as a virtual salt flux $H = S_{ref}F$ into the Arctic basin accompanied with a heat loss Q (Eldevik, 2014). A volume transport $U = -k\Delta\rho = k(\alpha\Delta T - \beta\Delta S)$ is balanced by the surface overflow. A

[4]The chosen values and details shown in table 2.1 are to support the theory given. A more detailed and extended review is provided in Stommel (1961) under Appendix on page 230.

MATLAB code provided by Professor Rune Wiggo Time was used to duplicate the Stommel model by simulation and see how freshwater forcing can determine a stable regime in the system. The basins shown in fig. 2.2 on page 6 are presented as pipes in the model. This parameter along side others such as pipe diameter, temperature, capillary tube length and diameter are varied to see how the freshwater influx effects the overturn, salinity change and density in the basins. The values of the mentioned parameters are gauged in accordance to the setup explained in chapter 3. Starting with the same parameters as shown on page 30, fig. 2.3 shows how the overturn and salinity change is affected by the freshwater influx. Given that the salinities in both basins are equal initially at $t = 0$, thermal differences dominate in the setup. Once the freshwater influx commences at $t > 0$, the density and salinity in the Atlantic basin will drop, hence the drop in the salinity change $\Delta S = S_1 - S_2$ below 0. A high bottom pressure at the Arctic basin will catalyse a positive overturn from the Atlantic to Arctic basin driven by a thermohaline circulation with an increase in salinity and density as shown in fig. 2.4 on the next page to the bifurcation point at $t = 0.3 \times 10^5$s. From $0.3 \times 10^6\text{s} < t < 0.6 \times 10^6$s, the salinities in both basins are no longer equal and the densities in both basins have plateaued implying a stable haline circulation. The overturn drops slightly during this period with a steady increasing F. The haline circulation is maintained until the freshwater influx F is stopped. If the F is stopped, this means there is no longer a pressure difference between the basins or a drop in ΔS due to a declining salinity and density at the Atlantic basin. Therefore, the haline circulation ceases and the thermal regime is reinstated at $t > 0.6 \times 10^6$ with a constant overturn, equal salinities and clear distinct density differences between the basins. An increase in pipe height and basin 2 (Arctic) temperature to

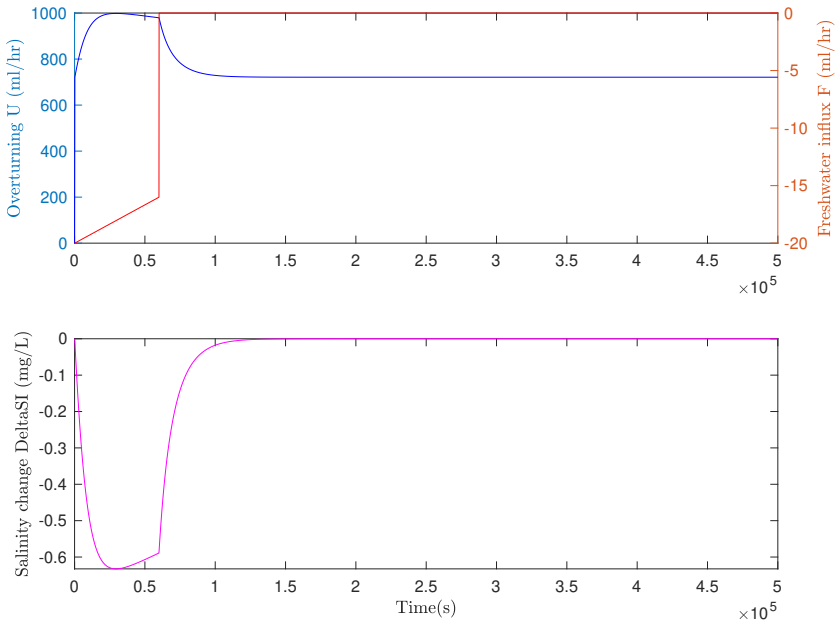

Figure 2.3: A loss of freshwater influx F contributes to a zero salinity change thus implying an end to a haline circulation.

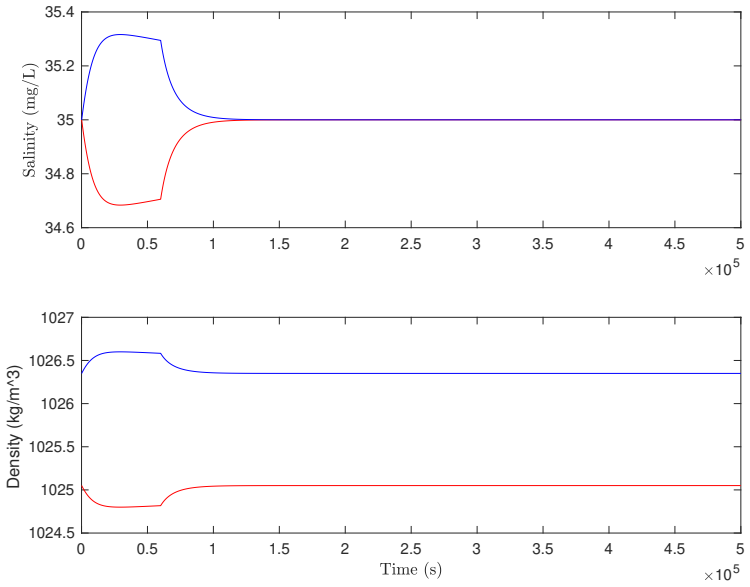

Figure 2.4: A zero salinity change generates equal salinity in both basins thus giving way to a thermal regime. Blue stands for basin 2 (Arctic) and red for basin 1 (Atlantic).

$5.190m$ and $T_2 = 14^*C$ respectively will generate a change in overturn as shown in 2.5, where the red dots indicate the return of a thermal regime for the overturn shown in figure 2.3 at $4m$ pipe length. An increase in temperature in basin 2 will generate a decrease in density and this will be the drawback in the overturn as shown in figure 2.5. Subsequently, also a drawback in the time span for a haline regime than previously. Moreover, ΔS and the salinity will be identical to that shown in figures 2.3 and 2.4, but with shorter and less steep time span for the haline regime.

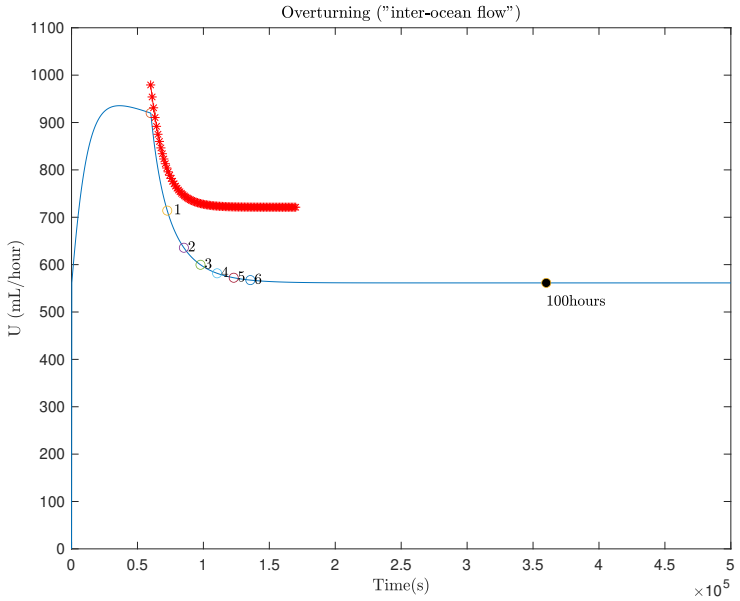

Figure 2.5: An increase in pipe and Arctic temperature generates a lower overturn. The red dots apply to the case of a $4m$ pipe height indicating a return to a stable thermal regime.

3 Experimental Setup

The idea of the experiment to duplicate TCH in the laboratory setup explained in the following chapter. The experiment is to examine the preservation of the salt content in the liquid. Ideally, the salt balance should be constant between the basins at termination of the experiment. The circulation system is two pumps representing the Arctic and Atlantic basin with different temperatures provided by the water baths in the temperature regulation system. The evaporation system duplicates the heat input to the Atlantic basin, whereas the salinity regulation system creates a salinity difference whilst keeping the salinity balance constant. Salinity and temperature sensors are calibrated before usage by following Appendix A on page 36. Data is collected using a control system called PASCO Capstone. Lastly, the flow through the pipes and capillary tubes is measuring by an upper and lower Sensirion flow meter.

3.1 The small scale rig setup

A silicone sealant is used to connect the acrylic pipes and the PVC transition couplings. The valves are connected to the acrylic pipes with PVC transitions and fittings screws. Two fluid systems are marked with different colors. The Atlantic Ocean is marked with red and the Arctic Ocean with blue. The valves also give a distinction between the two fluid systems. The pipe system is connected to aluminium profiles with nylon cable ties. Table 3.1 below shows the pipe dimensions along with descriptive figures of the setup and components. The figures 3.1 and 3.2 on the following page illustrate the dimensions given in table 3.1 below.

Table 3.1: Pipe dimensions for small scale setup. "w" stands for width and "h" stands for height.

Item	**Description**	**OD(mm)**	**ID(mm)**	**Length(mm)**
1	Acrylic pipe	50	40	155
2	Acrylic pipe	50	40	3940
3	Acrylic pipe	50	40	260
4	Acrylic pipe	50	40	970
A	PVC with 90° bend	-	50/40	$150 \times 165(wxh)$
B	PVC with T-coupling	-	50/40	$85 \times 155(wxh)$
C	PVC with 3-way valve	-	50/40	225 (w))
D	PVC with 2-way valve	-	50/40	140 (w)
E	Aluminium profile	90×90	-	5365
F	Aluminium profile	45×45	-	1020 (w)

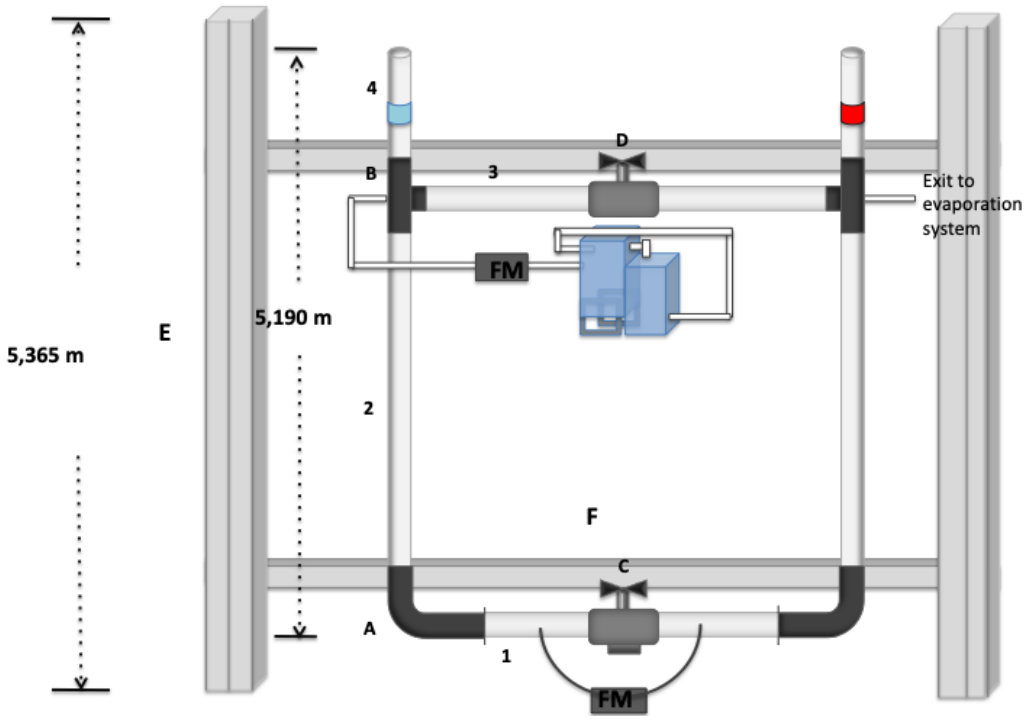

Figure 3.1: A detailed illustration of the preexisting small scale setup.

Figure 3.2: Valves and couplings used in the small scale setup.

3.2 Rig elements and systems

3.2.1 Circulation system

In order to imitate the natural phenomenon of ocean circulation, we need to have pumps. More particular, two PP3300 model VWR peristaltic pumps used to displace the system fluid in a pulsing manner. These are illustrated in fig. 3.8 on page 19 found in section 3.3. Another advantage is that such pumps are low maintenance and sporadically replaced. The rotational speed is 4-400 RPM and the direction of the stream can be reversed by changing on the rotor. Section 3.2.2 will explain why the flow direction of the ocean basins is opposite to each other. Furthermore, the circulation

system is complete with the addition of capillary tubes, elastic pipes and threaded nipple tubes. A 8.5mm hole is drilled in each of the PVC couplings to install the threaded nipple tubes and a thread sealing tape is used to prevent leakage. Additional longer capillary tubes and elastic pipes are used for communication between the top and bottom of the respective ocean basins, thus completing the circulation system.

3.2.2 Temperature regulation system

Given that the Arctic and Atlantic ocean have different temperatures, we need to situate a temperature regulating system together with the circulation system. Fluid from the circulation system via capillary tubes flows through heat coil wires immersed in an open heating bath circulator and thus exiting into the pipes. Each ocean basin has its respective water bath. The Arctic is set at 15°C[5] and the Atlantic at 20°C. Upper and lower valves are both closed when calibrating each ocean basin to its respective temperature. In the pipes, existing fluid is replaced with temperature calibrated fluid. Cold fluid replaces warm fluid in the Arctic ocean, while the opposite occurs in the Atlantic ocean. In order for both ocean basins to have the same replacement of fluid, the flow direction in the Atlantic is reversed, so that cold fluid replaces warm fluid as illustrated in fig. 3.3 on the next page.

3.2.3 Evaporation system

The evaporation system is stationed on shelves made of aluminium profiles placed separate from the main setup. The following are the components of the system as shown in fig. 3.4 on page 15:

1. A $2000W$ Wilfa hotplate with mechanical control from
    - A Powerstat $0 - 280V$ voltage regulator
    - A Co/Tech power meter
2. A $20ml$ glass flask situated inside a cylindrical glass with:
    - An entry from the Atlantic basin via a capillary tube and an exit to the replacement valve illustrated in fig. C.2 on page 45
    - A plastic cover with an outlet for vapor and an inlet for injection of air

Instead of using the mechanical control on the hotplate, an external voltage regulator is used for providing power to the hotplate. The regulator is connected to a power meter, thus to manage

[5]The mentioned temperature is refuted in section 4. The Arctic water bath was set to 14°C as explained in the mentioned section.

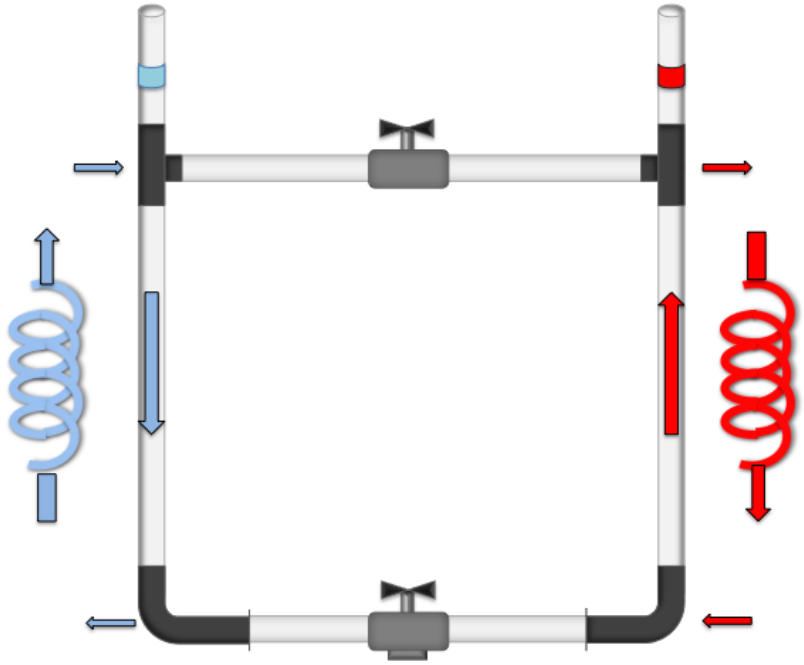

Figure 3.3: An illustration of the thermo regulation system. Notice how the direction of both flows is opposite to each other.

how much unit of power, also known as watt W, is supplied to the glass flask in the cylindrical glass on the hotplate. Pressure surrounding the cylindrical glass is the same pressure inside the glass flask, in other words the vapor pressure. If the water vapor is not effectively transported, in other words it is limited and confined in one space, the vapor pressure will reach the saturation pressure and this will restrict the evaporation rate. To counteract this problem, an injection point is found at the plastic cover, however there is a slight hurdle. Little or too much air can restrict the evaporation rate too! In section 3.2.4, an additional purpose of the evaporation system will be explained.

3.2.4 Salinity regulation system

The salinity regulation system as illustrated in fig. 3.5 on page 17 is a collection of the previous mentioned systems in addition to a buffer system. Below is a preview of the collection:

1. A buffer system consisting of
    - A Manson DC voltage regulator
    - Two plastic $4.6L$ water containers
    - A small In-line pump between the water containers using elastic pipes

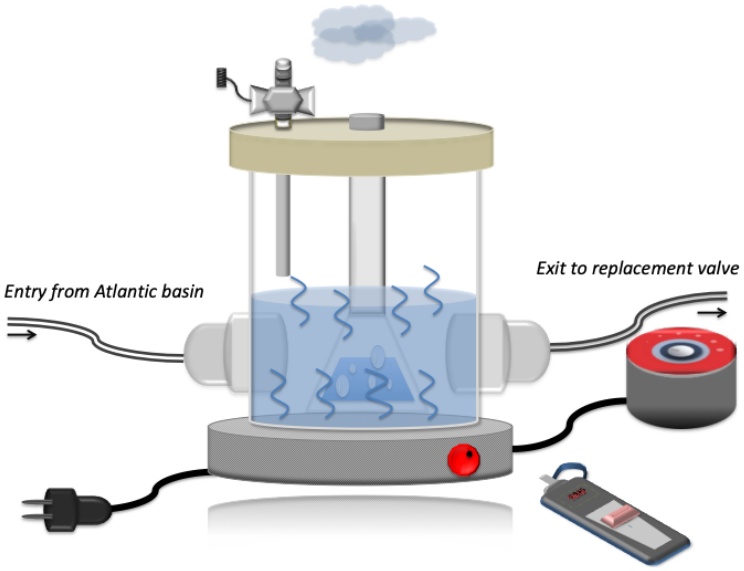

Figure 3.4: An illustration of the evaporation system.

- A flow meter at the exit to the Arctic basin

2. The evaporation system

3. The temperature regulation system

The previous section gives a thorough detailing about the evaporation system and the purpose of it is to create a salinity difference between the basins while keeping the salinity balance constant. This is achieved by supplying more salty water back to the Atlantic basin by evaporation of mentioned basin, while adding evaporated liquid to the Arctic basin as freshwater. The evaporated liquid will accumulate in the cylindrical glass generating increased salinity. A capillary tube is situated at the entry of the glass to supply salty water back to the Atlantic basin, while the exit entry of the glass is connected to a replacement valve. This acts as a barrier between the evaporation system (at the entry) and the temperature regulation system (at the exit to the Atlantic basin). The same driving force used in the circulation and temperature regulation system (the peristaltic pumps) is also used for the transportation of salty water. This force can be modulated by adjusting the opening of the valve.

However much the system is used to regulate the salinity, the following nuisances can occur:

1. The water level in the cylindrical glass falls

   - This will result in abnormally high readings of evaporation rates and also an indicator that the systems water level is too low in the buffer system. A more thorough detailing of the system is explained further down.

2. A depletion in evaporation rates

    - This indicates a mismatch between water supplied to the cylindrical glass and the evaporation rate. The increase in water is high thus energy supply from the hotplate is not sufficient enough.

3. Small openings in the replacement valve

    - As time passes, the water in the cylindrical glass will accumulate more and more salt. Moreover, the freshwater supply to the Arctic basin will have more leverage on the salinity difference between the basins, while the salty water supply to the Atlantic basin is significantly reduced. Thus, the mass balance of salt is void in the system.

As mentioned before, evaporated liquid is transported to the Arctic basin as freshwater via the buffer system. The water level in container 1 indicates the water level in the whole system before boiling takes place in the evaporation system. In other words, the Arctic and Atlantic basin, and the cylindrical glass level fluctuate at this level. The water level in the container 1 is 3.5L while the water level in container 2 fluctuates between $1 - 3$L. Both containers are marked with the levels. As evaporation takes place when boiling commences, the following processes occur:

(i) Salt accumulates in the glass flask as evaporated water disappears into the atmosphere as vapour.

(ii) Saltwater from the Atlantic basin is supplied to the cylindrical glass to balance the water level.

(iii) Saltwater is supplied from the Arctic to the Atlantic basin.

(iv) Freshwater is supplied from container 1 in the buffer system to the Arctic basin.

The process of boiling and evaporation is provisioned by the small in-line pump and container 2. Hence, the water level in container 1 is kept constant during the experiment. Furthermore, a decrease in water level in container 2 can determine the evaporation rates during the experiment. A depletion will indicate that the water level of the whole system is too low, thus abnormally high readings in the evaporation rates. Moreover, a flow meter is placed at the exit to the Arctic basin to regulate how much water is evaporated in the evaporation system.

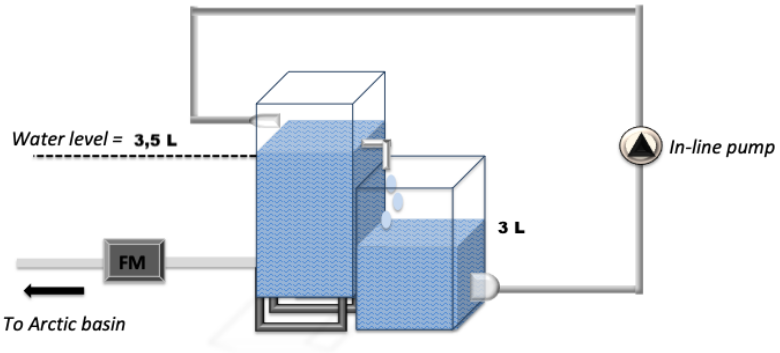

Figure 3.5: An illustration of buffer system included in the salt regulation system. Notice how the two tanks are at different levels. This is ensure flow through the capillary pipe due to gravity difference.

3.3 Measurement and control systems

Quantitative data from the experiment was collected by using measurement and control systems. PASCO 850 Universal Interface was purposely used to collect data from all sensors, while the Sensirion flow meters measured rates with both the upper and lower flow meter as shown in fig. 3.8 on page 19 together with the setup.

1. PASCO 850 Universal Interface used to measure temperature and salinity (conductivity). The instrument garners the following sensors:

   - 4 wired temperature sensors
   - 2 wireless temperature sensors
   - 2 wired PS-2195 conductivity sensors built with temperature measurement

   The sensors mentioned above are spread evenly along both poles of the setup. The Arctic and Atlantic basin are indicated with P and A respectively with descending numbering upwards, thus number 1 marks the top of the setup, while 4 labels the bottom. Sensors marked with 2 are connected via Bluetooth connection, while the remaining are connected to PASCO Interface via wiring. The PASCO Interface is then connected to a desktop and the software PASCO Capstone is used to gather data and visualize real-time data from the sensors as presented in chapter 4.

2. To Sensirion flow meters

   (i) **Lower flow meter**. It has a measurement interval from $-2500 < \mu\text{l/s} < +2500$ or in SI-units, $-150 < \text{ml/min} < +150$. A 3-three bypass valve is installed here and is kept closed during the experiment so that water streams through the flow meter. It

measures the overturn between the basins and in which direction this occurs as shown in fig. 3.6. Data is retrieved via a cable to a stationary desktop.

(ii) **Upper flow meter**. This has more constrained interval at $-65 < \text{ml/min} < +65$, where it is positioned between the buffer system and the upper region of the Arctic basin as shown in fig. 3.7. It measures the amount of freshwater transferred to the Arctic from the buffer system. In other words, the amount of freshwater gives an indication of the amount of vapor in the glass flask. A laptop is used to retrieve data from the flow meter. The positive flow is from the buffer system to the Arctic basin.

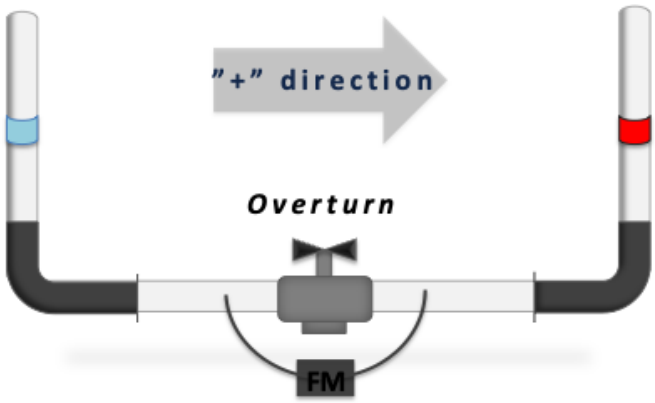

Figure 3.6: An illustration of the lower flow meter.

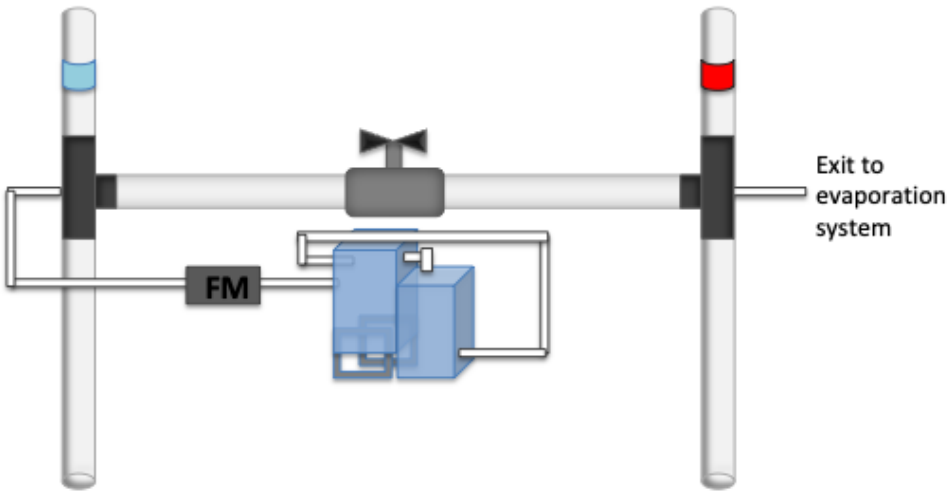

Figure 3.7: An illustration of the upper flow meter.

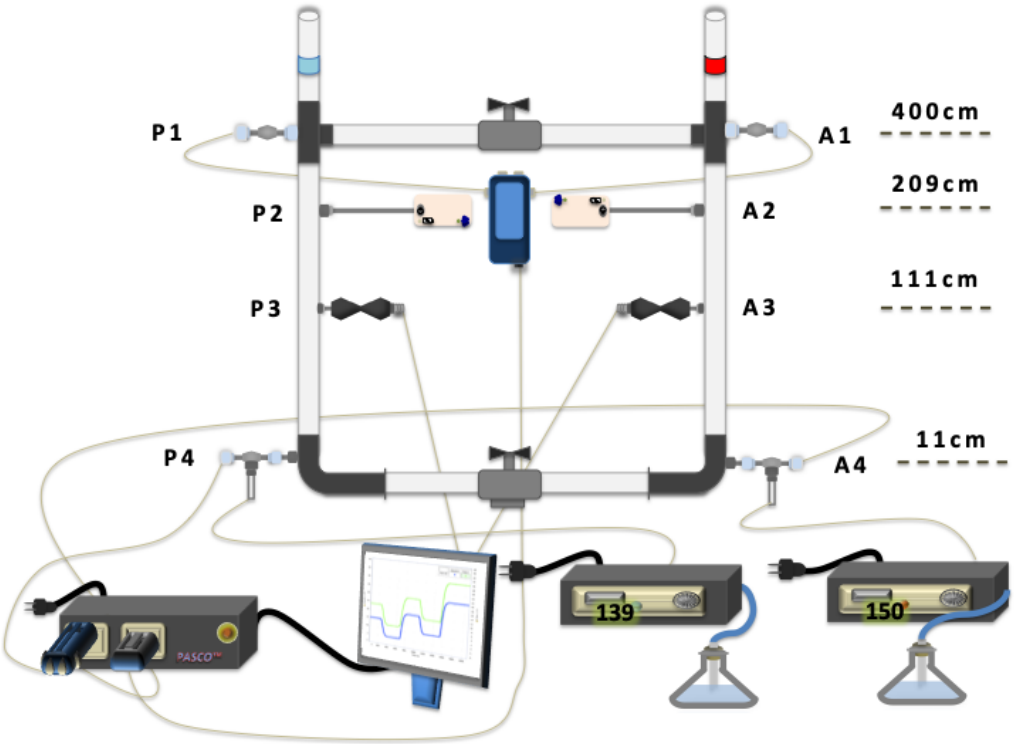

Figure 3.8: An illustration of the external measurement and control systems.. The Erlenmeyer flasks are replaced as shown in fig. C.1 on page 45. An explanation as to why is found in section 4.2 under chapter 4.

4 Results and discussions

The following chapter showcases solutions from calibrations before the experiment and results from the experiment. During multiple thermal runs, alterations were performed on sensors A4 and P4 as shown in figure C.8on page 48 due to multiple, unwanted peaks in the data readings recorded by PASCO. In the midst of preparing for the experiment, a number of observations were noted which are mentioned in the beginning of section 4.2. Circumstances were met during the proceedings of the experiment, however, this did not discourage an end result, where the salt content was not at 35 ppt as expected.

4.1 Solutions from calibrations and test runs

(a) **Temperature sensors.** Judging from the figures C.3, C.4 and C.5 on page 46 and 47, the Arctic sensors are well above 15°C. The temperature of the Arctic basin was first set at 15◦C, however this was refuted during the process of calibration and later changed to 14°C. The figures also show that there are a lot of peaks and for that reason calibrations were performed.

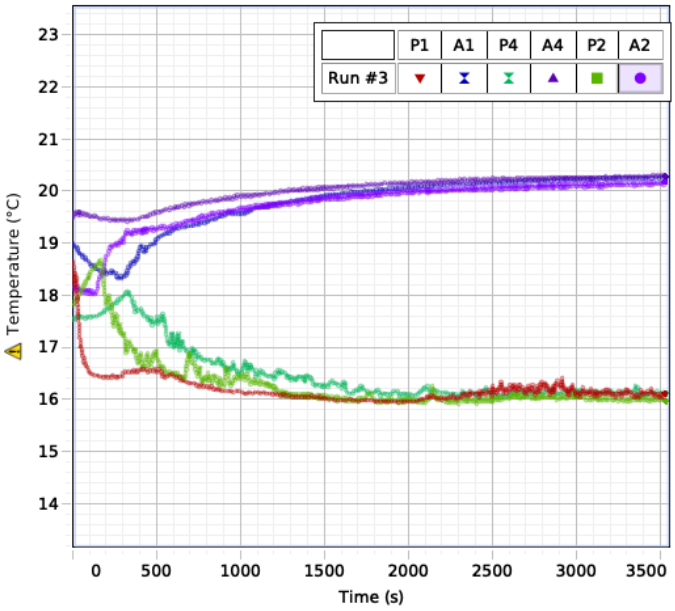

Figure 4.1: First run after calibration before changing Arctic basin temperature with the upper valve closed.

The calibration method mentioned the beginning of (a) on page 36, shows the following results after the first thermal run in figure 4.1 above. Peaks are still an occurrence well until the second run. During the second run, water bath temperature was lowered for the Arctic basin and the bottom Atlantic sensor (A4) malfunctioned, as figure C.6 on 47 illustrates. The sensor was replaced and the third run was continued the next day. The latter part of (a) on page 36 was executed during the third thermal run after calibration as shown in figure 4.2 on 21. All Arctic sensors are perfectly aligned on 15°C and there are no evident disturbances. The Atlantic sensors use a longer time period to reach their assigned temperatures compared to the Arctic sensors, which stabilize at 15°C by approximately 16 minutes. All test runs were controlled for an hour each. It was noted during multiple thermal runs, sensors A4 and P4 were out of their normal temperatures regions accompanied multiple, unwanted peaks and it was thought that lowering the RPM at both basin would eliminate the inconsistencies, which are not illustrated in this thesis. However, the issue was solved by inserting a small plastic pipe as shown in fig. C.8 on page 48.

(b) **Salinity sensors.** The readings from the calibration solution after following the steps explained in (b) on page 37 are shown in table 4.1 on page 22. According to fig. 4.3 on the following page the readings are aligned on the trend line after averaging the values. The formula shown is the same formula used throughout the main experiment, as explained in (b).

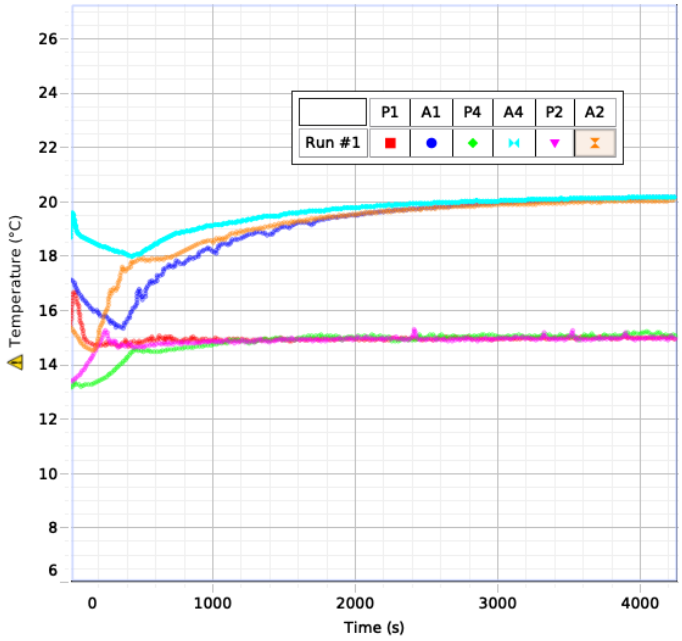

Figure 4.2: Third run after proper calibration, replacing defect A4 sensor and lowering Arctic water bath temperature.

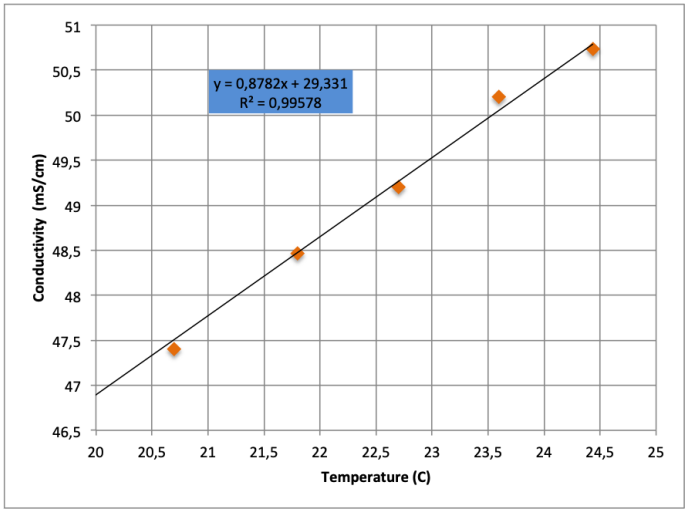

Figure 4.3: Mettler Toledo values of calibration solution after averaging. An increase in the R^2-number compared to figure C.7 on page 48.

(c) **Powerstat voltage regulator.** The voltage regulator was found to be in correlation between the change in intensity supplied by the power meter considering the logarithmic graph in fig. 4.4 on the next page. A logarithmic scale is chosen due to the wide range of values in both voltage and intensity.

Table 4.1: Mettler Toledo readings of the calibration solution after averaging.

Temp [°C]	**Cond [μS/cm]**
24.43	50.73
23.6	50.2
22.7	49.2
21.8	48.46
20.7	47.4
19.9	46.9

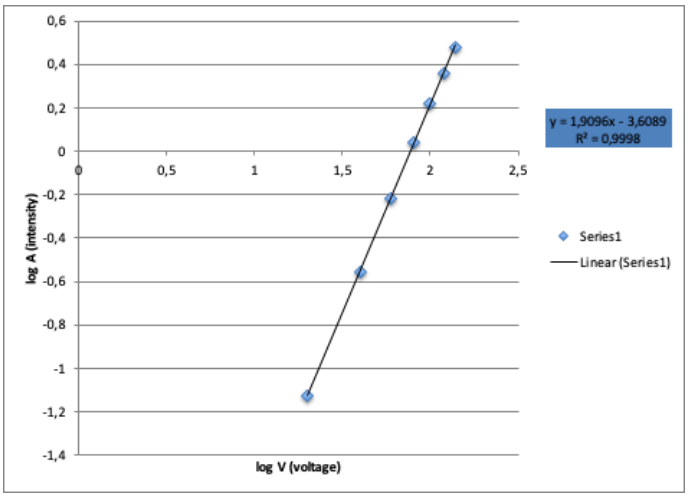

Figure 4.4: Logarithmic scale of the voltage and intensity from the regulator and power meter respectively.

4.2 Solutions from the experiment

The following section contains results from the experiment along side discussions. The test conditions are $14°C$ and $20°C$ for the Arctic and Atlantic basin respectively. The observations expected from the experiment are to connect with the theory presented in chapter 2. It is expected that a freshwater influx (at $t > 0$) will create a salinity difference between basins in the setup therefore having an overturn driven by a thermohaline circulation. Once the freshwater influx is stopped, it is expected that the salinity in both basins to be equal (as they are at $t = 0$) thus returning to a thermo regime. In other words, we are to except a mass balance of salt content in the mixture. The experiment is conducted for 4.5 hours excluding the time prior used by the upper flow meter to determine the consistency of the water level in the setup. The results are presented with alternative outcomes than those given in the some figures in order for the reader to understand

that despite the mishaps in the results, the main task is to examine whether or not a mass balance in salt content is maintained at the end of the experiment. Suggestions for improvement will be presented lastly.

Recalling the alignment of the temperature sensors in fig. 3.8 on page 19, allocated data points from the sensors during the experiment are shown in fig. 4.5 by using the measurement system PASCO Capstone. The addition of a plastic pipe around sensors $P4$ and $A4$ shown in fig. C.8 on page 48 has improved their performance, however all sensors have a presence of oscillations with $P1$ having the most. This comes from the fact that the temperature sensors (except for $P3$ and $A3$) are highly sensitive thin wired probes.

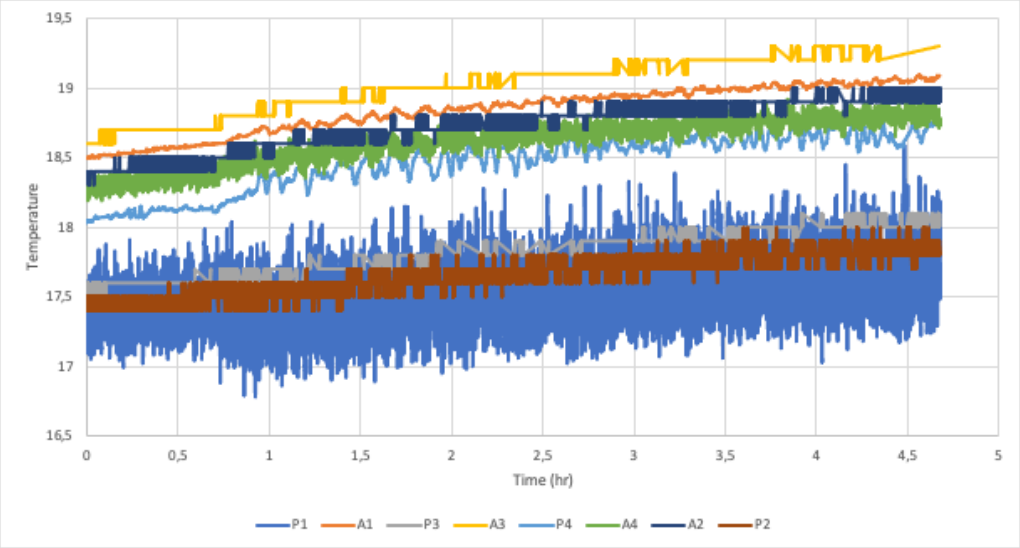

Figure 4.5: The behaviour of temperature sensors during the experiment proved to show how sensitive they are. Notice how $P1$ has the most disturbances, which can be due to the massive down flow passing the sensor as it is situated near the upper flow meter.

Before starting the allocation of data points via PASCO Capstone, both the upper and lower meter were started one hour and half before connecting the power supply as shown in fig. A.1 on page 40 and starting the experiment. Stable readings of 0.2–0.5 ml/min through the upper flow meter indicate a constant water level in the setup. Nonetheless, the upper flow meter in fig. 4.6 on the following page shows reading way below this range despite the fact that the water level was constant. Upon starting the experiment, the freshwater input is negative implying a flow from the Arctic basin to the buffer system the opposite of that depicted in fig. 3.5 on page 17. This incident is quite negligible as it does not take long before it is reversed with positive flow values suggesting flow as that illustrated in fig. 3.5 on page 17. Once the maximum supplied power is reached at 700 W, at approximately 50 minutes after start of the experiment, the freshwater input reaches a plateau at 2.7–4.5 ml/min, which is equivalent to 210–240 ml/hr. The plateau stage will end

once power supply is terminated thus creating a drop in freshwater input. The curve will decrease further until it stabilizes around 0 because of balancing of the water level in the system marking the end of the experiment. Remarkably, the range at which the upper flow meter operates, is quite small judging from the figure. This range can expand provided that the power supply is increased, but not considerably much.

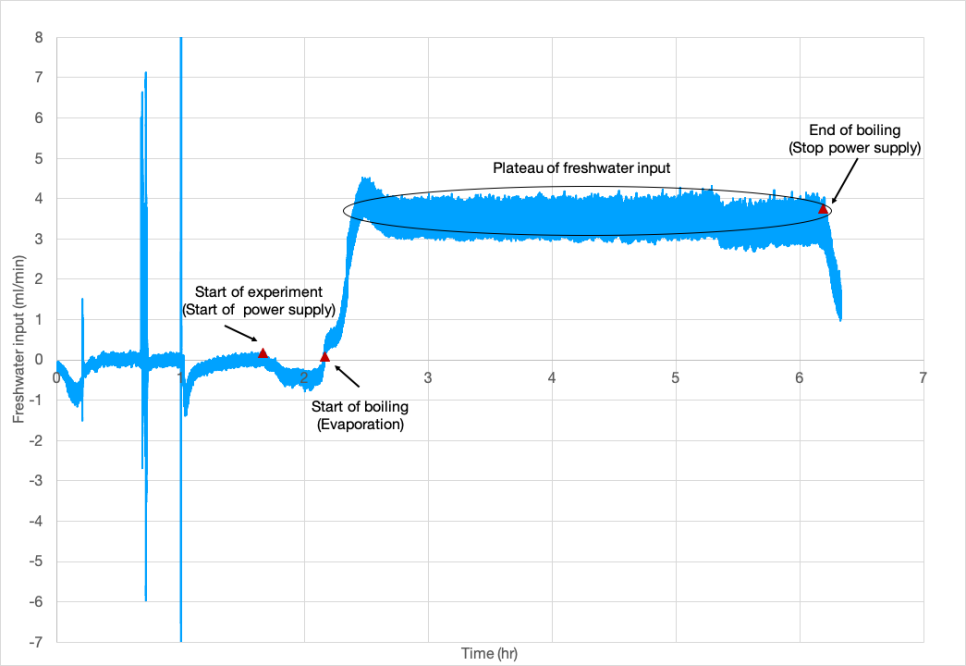

Figure 4.6: The flow of the freshwater input in the upper flow meter. The peaks prior to the start of the experiment are due to pressing of capillary tubes at the flow meter. The y-axis is shortened for detail.

On the contrary, the flow range of the lower flow meter is considered much wider as the overturn is dependant on both the temperature and salinity differences in the system. The flow range can lay between -200–500 μl/s. However, judging from fig. 4.7 on the next page this is not the case. Ideally[6], the overturn should rapidly rise at the start of the experiment until evaporation. Since the salt mixture is fairly the same at start, the temperature differences would dominate the overturn with a flow from the Arctic to the Atlantic basin. A plateau will commence between evaporation and the beginning of the freshwater plateau. Beyond this, a pull between salinity and temperature dominance will occur until the overturn drops below x-axis indicating flow from the Atlantic to the Arctic. In other words, the salinity differences will define the overturn. Once the power supply to the evaporation system is cut off, the overturn will gradually grow towards positive values as the freshwater input diminishes. Hence, the saltwater flows back to the Arctic from the Atlantic

[6]When using the word "ideally", it is correspond to the behaviour of the freshwater input through the upper flow meter in figure 4.6.

basin. By the time the freshwater input is below the x-axis, the overturn is again dominated by temperature differences and flow is from the Arctic to the Atlantic basin.

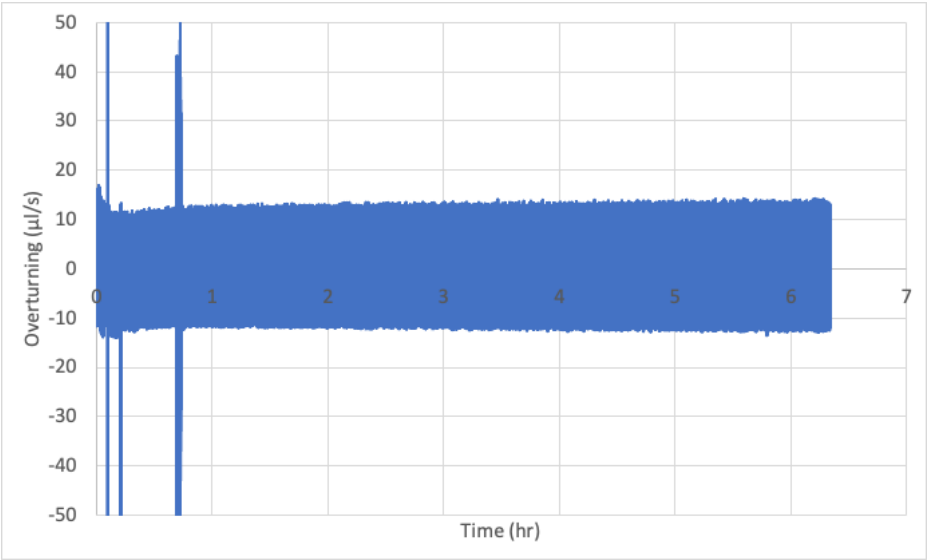

Figure 4.7: Overturn flow in the lower flow meter. There is no indication of any flow through the flow meter even after thorough inspection of the system insuring no blocked passages.

Following the same reasoning, the conductivity in the respective basins should ideally[6] contrasting than that illustrated in fig. 4.8 on the next page. Recalling that the salt solution prepared is 35 ppt (**53.0065 mS/cm**), the averaged conductivity measurements in the evaporation system (fig. 3.4 on page 15) was **182.13 mS/cm** compared to **49.82 mS/cm** and **47.91 ms/cm** at the Arctic and Atlantic basin respectively at the end of the experiment. These values indicate a diminishing salt content in both basins and a salt accumulation in the evaporation system. Therefore preservation of mass balance in terms of salt content is not maintained. Furthermore, a totalizer of 821.51ml salt mixture flowed through the upper flow meter salt mixture during the 4.5 hour experiment, meaning it total amount of evaporated liquid. As mentioned in the beginning of this section, despite the mishaps in some results, a final result was however retrieved from the experiment. Considering the results alone (without looking at the alternative ones given), we can see a dynamic temperature and salinity in the system. Therefore making it difficult to determine which of the two drives the overturn. Given that both properties are dynamic, it is maybe no surprise that the overturn does not vary at all in fig. 4.7. Recalling the probing question as to how an external agent can stabilise a circulation mode on page 8, it it evident how freshwater input can stabilise a circulation mode. Transitions between the circulation modes can be considered abrupt given that the first transition happened less than half of the time spent on the experiment.

As a suggestion to eliminate the issue of salt accumulation, the replacement valve (fig. C.2 on

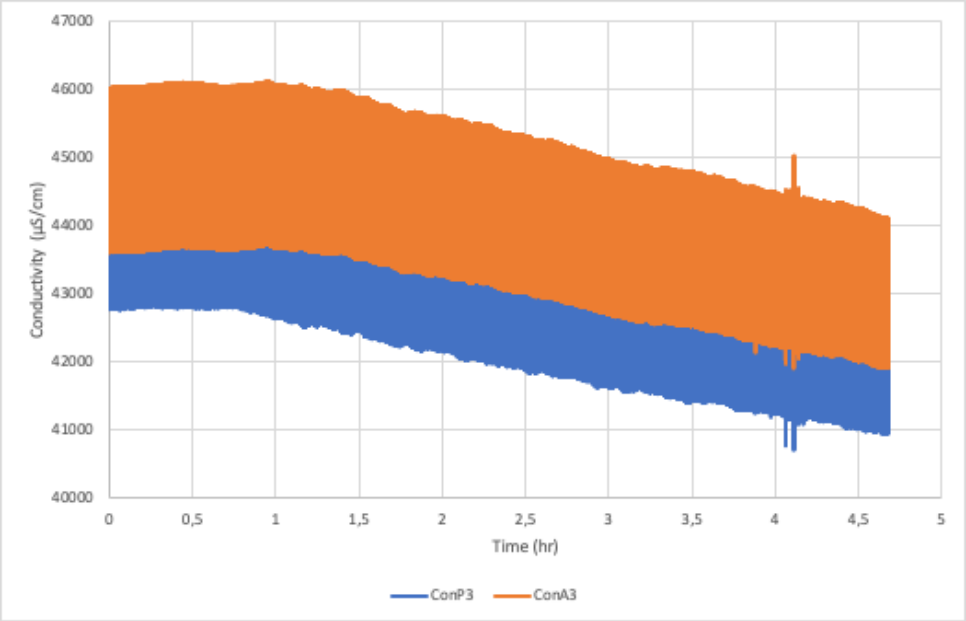

Figure 4.8: The conductivity in both basins follow each other. From the figure, we see that 40 min after start, the conductivity in both basins drops.

page 45) can maybe be kept open during the experiments. However this raises can issue where the water level in the evaporation system (fig. 3.4 on page 15) will raise because of the inflow from the Atlantic basin. Hence the power supplied might not be sufficient enough to generate an optimal evaporation rate with raising water levels. The power supply to the evaporation system could be reduced along with a lower RPM on both basins, thus shortening the occurrence of salt accumulation. However, this means a longer time duration for evaporation to happen and thus a longer time duration for the entire experiment. Another suggestion would be placing the replacement valve at a higher level than the evaporation system thus ensuring that additional flow into the glass flask is limited. Additionally, the salt content could be filled halfway in the upper horizontal pipe to ensure a better overflow, but this will create an imbalance between the water level in the glass flask and the Atlantic basin. The water level will diminish in the glass flask thus refuting the task of having a constant water level during the experiment. Furthermore, adding a subsection of coding about the evaporation system to the MATLAB code on page 30 provided by Rune Wiggo Time (UiS) be used to examine the issue or construct a medium scale setup to compare the results from the setups and see why the issue arises. Besides from the Stommel model, a simplified model of the THC shown in figure 5.1on the next page is simulated in the STELLA© software primarily used to examine abrupt climate change. Given that external systems like those detailed in chapter 3 are not needed, this can eliminate the issue of excessive salt accumulation. And finally, in terms of the oscillators in the temperature sensors, the white probes can be replaced with robust metal sensors.

5 Conclusions

The small scale setup described in chapter 3 takes into account the Stommel model (1961) to explain the thermohaline circulation between the Arctic and Atlantic ocean. Given the complexity and diversity of the THC, pinpointing a definite answer as to how it operates with the basis of results given in chapter 4 would be a miscalculation to say the least. Just as the Stommel model is used a preliminary, the results garnered so far can be used to acknowledge the intricacies of the THC. The NORTH project examines such aspects of the thermohaline circulation including how climate change and feedback can effect the circulation. An example of such a feedback is a freshwater input at the Arctic basin, where it was evident that it has a maximum value generating a change in direction in terms of the overturn thus creating a salinity dominance. In other words, an increase in precipitation increases the salinity. However, results show how the salt accumulates in the evaporation system indicating an ineffective flow of the salt content to the Atlantic basin. An effective movement from the glass flask in the evaporation system will create an overturn earlier thus a freshwater input plateau much earlier than that shown in fig. 4.6 on page 24. Therefore a return to temperature dominated circulation is reinstated earlier. Suggestions on how to improve the setup are given in the previous chapter, however these do have some limitations aside from the one mentioned about the STELLA© shown in fig. 5.1. In conclusion, despite the shortage of complimenting results, this thesis can be used as a precursor to better the experimental setup and further examine the inefficiency in salt drive to the Atlantic.

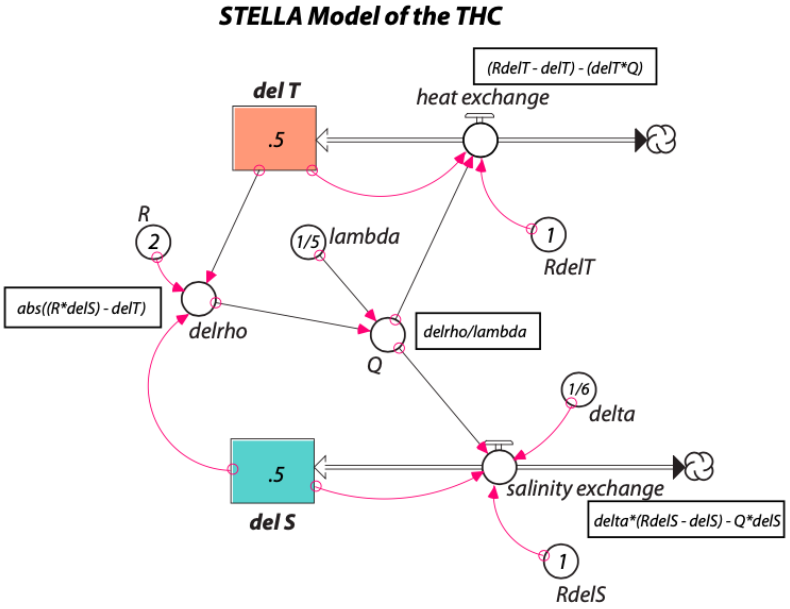

Figure 5.1: A simplified model of the THC simulated in STELLA© software primarily used to study abrupt climate change.

References

Cheng, Wei et al. (2018). "Can the Salt-Advection Feedback Be Detected in Internal Variability of the Atlantic Meridional Overturning Circulation?" In: *Journal of Climate* 31.16, pp. 6649–6667.

Eldevik, Tor (2014). "A note on Stommel's box model and its extension to the Arctic Mediterranean (in progress)". In:

Encyclopedia (n.d.). *Ocean and Continents: Gulf Stream*. `shorturl.at/fmLM1`. Accessed on April 20th, 2020.

Guan, Yu Ping and Rui Xin Huang (2008). "Stommel's box model of thermohaline circulation revisited—The role of mechanical energy supporting mixing and the wind-driven gyration". In: *Journal of physical oceanography* 38.4, pp. 909–917.

Hawaii Pacific University, Oceanic Institute (n.d.). *Aqua facts*. `shorturl.at/muHT0`. Accessed on February 18th, 2020.

Lambert, Erwin, Tor Eldevik, and Peter M Haugan (2016). "How northern freshwater input can stabilise thermohaline circulation". In: *Tellus A: Dynamic Meteorology and Oceanography* 68.1, p. 31051.

Lohmann, Gerrit and Rüdiger Gerdes (1998). "Sea ice effects on the sensitivity of the thermohaline circulation". In: *Journal of Climate* 11.11, pp. 2789–2803.

Motion, Ocean (n.d.). *Wind Driven Surface Currents: Gyres Background*. `shorturl.at/noGR4`. Accessed on April 20th, 2020.

Munk, Walter and Carl Wunsch (1998). "Abyssal recipes II: Energetics of tidal and wind mixing". In: *Deep-sea research. Part I, Oceanographic research papers* 45.12, pp. 1977–2010.

Oka, A, H Hasumi, and N Suginohara (2001). "Stabilization of thermohaline circulation by wind-driven and vertical diffusive salt transport". In: *Climate dynamics* 18.1-2, pp. 71–83.

Otterå, Odd Helge and Helge Drange (2004). "A possible feedback mechanism involving the Arctic freshwater, the Arctic sea ice, and the north Atlantic drift". In: *Advances in Atmospheric Sciences* 21.5, pp. 784–801.

Rahmstorf, Stefan (2006). "Thermohaline ocean circulation". In: *Encyclopedia of quaternary sciences* 5.

– (n.d.). *The Thermohaline Circulation*. `shorturl.at/fNSY2`. Accessed on May 31st, 2020.

Rennermalm, Asa K et al. (2006). "Sensitivity of the thermohaline circulation to Arctic Ocean runoff". In: *Geophysical research letters* 33.12.

Research Center, Smithsonian Environmental (n.d.). *Arctic Meltdown*. `shorturl.at/bmxz8`. Accessed on May 31st, 2020.

Robinson, Allan and Henry Stommel (1959). "The oceanic thermocline and the associated thermohaline circulation 1". In: *Tellus* 11.3, pp. 295–308.

Stommel, Henry (1961). "Thermohaline convection with two stable regimes of flow". In: *Tellus* 13.2, pp. 224–230.

Stommel, Henry and Claes Rooth (1968). "On the interaction of gravitational and dynamic forcing in simple circulation models". In: *Deep sea research and oceanographic abstracts*. Vol. 15. 2. Elsevier, pp. 165–170.

Toggweiler, JR and B Samuels (1993). "Is the magnitude of the deep outflow from the Atlantic Ocean actually governed by Southern Hemisphere winds?" In: *The global carbon cycle*. Springer, pp. 303–331.

Walin, Gösta (1977). "A theoretical framework for the description of estuaries". In: *Tellus* 29.2, pp. 128–136.

– (1982). "On the relation between sea-surface heat flow and thermal circulation in the ocean". In: *Tellus* 34.2, pp. 187–195.

Walsh, James (2019). "The Ocean and Climate Change: Stommel's Conceptual Model". In: *CODEE Journal* 12.1, p. 3.

Webb, Paul (2019). *Introduction to Oceanography*. Pressbooks.

Whitehead, JA (2009). "Abrupt transitions and hysteresis in thermohaline laboratory models". In: *Journal of physical oceanography* 39.5, pp. 1231–1243.

Matlab code - by Professor Rune Wiggo Time (UiS)

```
% ********************************************
% External function call: "density_Stommel(S,T).m"
% ********************************************

clc
clear all
format compact
clf

' '
'LAB data'
'********'
% Input data:
g = 9.81
% Salinity model constants
Alfa = 1.3e-4 % K^-1
Beta = 7.9e-4 % Non-dimensional numbers alfa and beta
my = 1e-3      % Water viscosity, cP

D = 4e-2   % Vertical pipes diameter m
Height = 4 % Pipe height m

Areal =(pi*D^2/4) %Pipe cross section
Volum =Areal*Height % Volume per pipe
V = Volum %m^3

% Capillary crossover tube (at Sensirion flowmeter)
dcap = 2e-2     % 2e-2 % diameter (m)
lcap = 1 % 1.0 % Length of capillary tube
arealc=pi*dcap^2/4

% Flow contant k
k=Height*g*arealc*dcap^2/(lcap*32*my)

% Time constant example
```

```
T1=20 %degC
T2=10
% T1=17 %degC
% T2=13
DeltaT=T1-T2
% Time constant Tauc accrding to Stommel-Eldevik:
invTauc=2*k*Alfa*DeltaT/Volum
Tauc = Volum/(2*k*Alfa*DeltaT)
Tauc_hours=Tauc/3600
%Check that k is correct for equal salinities
S1=35
S2=35
Sref=(S1+S2)/2
DeltaS=S1-S2
rho1=density_Stommel(S1,T1)
rho2=density_Stommel(S2,T2)
Drho=rho1-rho2
DP=Drho*g*Height % Pressure difference between "Atlantic" and "Polar"
                 % at the bottom of the two pipes
q1=-k*Drho
q2=-(DP/lcap)*(dcap^2/(32*my))*arealc

% RHO1=density(S1,T1)
% RHO2=density(S1,T2)
% DRHO=RHO1-RHO2

Dpdx=DP/lcap
Q=-Dpdx*(dcap^2/(32*my))*arealc
kny=-Q/Drho
k=Height*g*arealc*dcap^2/(lcap*32*my)

% Simulation time data
Time(1)=0
dt=100      % Time interval between each calculated value (seconds)
Imax=5000 % dt*Imax gives max simulated experiment time
Tmax=dt*Imax
```

```
% Data for triangular pulse
Fmaxmlperhour=20 % Predefined amplitude - mL/hour
Fmax=Fmaxmlperhour*1e-6/3600 % m^3/s
dFmlperhour=Fmaxmlperhour/3000    % mL/hour per time step
dF=dFmlperhour*1e-6/3600 % m^3/s
F(1)=-Fmax

% ************************

H(1)=Sref*F(1)

% hkonstml=1 % in ml/s
% hkonst=hkonstml*1e-6 % m^3/s
SI1(1)=S1
SI2(1)=S2
omega=0.001 % For sinusoidal oscillation
DeltaSI(1)=DeltaS;

itype = 2
for i=2:Imax    % **** START TIME LOOP AND PULSING ********
    Time(i)=i*dt;
    U(i)=k*(Alfa*DeltaT-Beta*DeltaSI(i-1));
    switch itype
        case 1
            F(i)=0.96*sin(omega*Time(i))+1; % Sinusoidal freshwater
                pulse
        case 2
            F(i)=F(i-1)+dF;  % Tiangular freshwater pulse, start
                             % linear increase per timestep
            if F(i)>Fmax | F(i)<-Fmax  % Reverse the flow when max is
                reached
                dF=-dF;
            end
    end
%     %Eventually turn off freshwater forcing at Stopfresh;
Stopfresh = 60000;
```

```
    if Time(i)>Stopfresh %60000 (Note :  there are 3600 seconds per
        hour)
        F(i)=0;
    end
    % Equations derived from Eldeviks notat
    H(i)=Sref*F(i);
    %     DeltaSI(i)= DeltaSI(i-1)+dt*2*(H(i-1)-abs(U(i-1))*DeltaSI(i-1)
        )/Volum;
    DeltaSI(i)= DeltaSI(i-1)+dt*2*(H(i)-abs(U(i))*DeltaSI(i-1))/Volum;
    SI1(i)=Sref+DeltaSI(i)/2;
    SI2(i)=Sref-DeltaSI(i)/2;
    rho1(i)=density_Stommel(SI1(i),T1);
    rho2(i)=density_Stommel(SI2(i),T2);
end      % **** STOP TIME LOOP ********

figure(1)
Fmlpersec=F*1e6*3600; % Freshwater forcing
% plot(Time,F) % F in m^3/s
plot(Time,Fmlpersec) % F converted into mL/hour
hold on
tekst = 'Freshwater forcing stopped'
text(Stopfresh,-2, tekst)
xlabel('Time(s)')
ylabel('Freshwater flux F')
title('Freshwater forcing (mL/hour)')
axis([ 0 Tmax -25 2])
hold off

figure(2)

Umlpersec=U*1e6*3600; % "Overturning" - U is in m^3 per seconds
% plot(Time,U) % U in m^3/s
plot(Time,Umlpersec) % U converted into mL/hour
xlabel('Time(s)')
ylabel('U (mL/hour)')
title('Overturning ("inter-ocean flow")')
axis([ 0 Tmax 0 1100])
```

```
hold on

plotpoints=1
if plotpoints==1 %Plot points on the curve for multiples og time
    constant tc
tc=126;
plot(Time(600),Umlpersec(600),'o')
plot(Time(600+tc),Umlpersec(600+tc),'o')
text(Time(600+tc+50),Umlpersec(600+tc),'1','HorizontalAlignment','Left'
    )
plot(Time(600+2*tc),Umlpersec(600+2*tc),'o')
text(Time(600+2*tc+30),Umlpersec(600+2*tc),'2')
plot(Time(600+3*tc),Umlpersec(600+3*tc),'o')
text(Time(600+3*tc+30),Umlpersec(600+3*tc),'3')
plot(Time(600+4*tc),Umlpersec(600+4*tc),'o')
text(Time(600+4*tc+30),Umlpersec(600+4*tc),'4')
plot(Time(600+5*tc),Umlpersec(600+5*tc),'o')
text(Time(600+5*tc+30),Umlpersec(600+5*tc),'5')
plot(Time(600+6*tc),Umlpersec(600+6*tc),'o')
text(Time(600+6*tc+30),Umlpersec(600+6*tc),'6')
end

iexp = 1 % 1: Make plot of exponential curve fitted to the special case
         % described inirtially. If 0: skip
if iexp==1
% Plot an exponential curve in the same figure, just to see if there is
% similarities in behavior
it =linspace(6,17,100);
tid=it*1e4;
gamma=0.93;
Y = 721.2+(979.3-721.2).*exp(-gamma*(tid-6e4)/1e4);
plot(tid,Y,'-*r')
end

for iti=1:1
plot(3600*100*iti,Umlpersec(3600*iti),'o','MarkerfaceColor','k')
tekst=[ int2str(iti*100) 'hours']
```

```
text(3600*100*iti,Umlpersec(3600*iti)- 40 ,tekst)
end
hold off

figure(3)
plot(Time,DeltaSI,'-r')
xlabel('Time(s)')
ylabel('Salinity change (mg/L)')
title('Salinity change (mg/L)')
axis([ 0 Tmax -1 0.1])

figure(4)
plot(Time,SI1,'-r')
title('Salinity (mg/L)')
hold on
plot(Time,SI2,'-b')
xlabel('Time(s)')
ylabel('Salinity (mg/L)')
axis([ 0 Tmax 34.6 35.4])
hold off

figure(5)
plot(Time,rho1,'-r')
hold on
plot(Time,rho2,'-b')
xlabel('Time(s)')
ylabel('Density(kg/m^3)')
title('Density(kg/m^3)')
axis([ 0 Tmax 1024.5 1027])
hold off

function rho = densityStommel(S,T)
% Function for water density versus temperature and salinity (g salt/kg
    vann)
Alfa = 1.3e-4; %K^-1
Beta = 7.9e-4; % Non-dimensional
rho0 = 1000;
rho = rho0*(1-Alfa*T+Beta*S);
```

A Procedures

Preliminary procedures

Salt mixture and calibration solution A salt mixture known as the test/experiment liquid was prepared before considering the next sections. The mixture accumulated 15L by using a 5000ml volumetric flask with the following steps:

- Measure 33.03g/l water. This amounts to 165.15g NaCl per 5000ml volumetric flask
- Use a funnel and tube to deposit the salt into the flask
- Fill the flask halfway and mix
- Fill the flask to the marking. Be careful to use a small beaker for control
- Repeat the steps 3 times
- The mixute is stored in a 10l bucket and a 5000ml volumetric flask

Furthermore, a calibration solution is also prepared before accessing the salinity sensors. The solution has a value of 35ppt at 25°C, which equates to 33.03g of salt per liter water. It is stored in a 1000ml volumetric flask.

Calibrations Calibrations were performed before the main experiment to ensure accuracy and minimal error readings before the main experiment. These were done mainly on the temperature and salinity sensors, and the Powerstat voltage regulator used in section 3.2.3 on page 13. In terms of the flowmeters explained in section 3.3 on page 17, this step was not performed as these are delivered fully calibrated.

(a) *Temperature sensors.* Before concluding with implementing the calibration method below, another practice was used, which did not deliver desirable results. The method did not include steps performed in PASCO Capstone, like the following method does. Two calibration temperatures 10°C and 30°C were chosen on FLUKE. Each sensor was inserted into FLUKE one by one while being connected to PASCO Interface. In the PASCO Capstone software, the option of calibration is chosen and the type of measurement to be calibrated is selected (1). Furthermore, a 2 standard (2 point) calibration (2) was selected. At the first point, FLUKE was set at 10°C. The sensor readings (current valve) were let to stabilize for 10 minutes and the final reading from PASCO Capstone was entered as the standard value. Finally, the tab "Set Current Value to Standard Value" was selected (3). The same steps were repeated for the second point at 30°C.

(b) *Salinity sensors.* The setup is filled with the test solution and it left to stay overnight, so that it is approximately room temperature. Before calibrating the salinity sensors, an instrument used to measure the salinity has to calibrated first. The Mettler Toledo conductivity meter comes with manufactured solutions for calibrations with the following values 12.88mS/cm and 1413μS/cm. Each solution has it own specific values are given temperatures as shown in Table A.1 on the following page. A standard temperature of 25°C for the meter was chosen. While calibrating, it is essential that the readings from the meter are within the error range of the chosen solution. Furthermore, the calibration solution was poured into a 250ml Erlenmeyer flash and submerged into a water bath set at a temperature range of $20 - 25$°C. At each temperature step, readings of temperature and salinity of the Mettler Toledo conductivity meter were registered thrice in Microsoft Excel. The readings were averaged and a scatter plot was made in Excel together with a formula, where x is the measured temperature (°C) and y is measured conductivity (μS/cm).

$$y = ax + b$$

A thermo run was performed on the setup to register the temperature at both poles. Both valves were open and pumps were not running. Moreover, the salinity sensors were connected to PASCO Interface and selected one by one in PASCO Capstone. The calibration option is chosen and the type of measurement (1) is selected. One of the sensors is chosen (2) and the 1 standard calibration (1 point slope) (3) is selected. With the formula retrieved from Excel and the measured temperature determined for each pole, the conductivity y can be measured and chosen as the standard value. Thus, ending the calibration by pressing the tab "Set Current value to Standard Value" (4). Before doing this, it is essential that the current value readings are stabilized. The same steps are performed for the last sensor. The same formula is used, however, the temperatures must be measured before each experiment.

Table A.1: Conductivity standard values for manufactured Mettler Toledo solutions.

Temp [°C]	**[mS/cm]** ±1.5%
0	7.15
5	8.22
10	9.33
15	10.48
20	11.67
25	**12.88**
30	14.12
35	14.12

(a) A 12.88mS/cm solution.

Temp [°C]	**[μS/cm]** ±1.5%
0	770
5	896
10	1020
15	1147
20	1278
25	**1413**
30	1552
35	1696

(b) A 1413μS/cm solution.

(c) *Powerstat voltage regulator.* Since the evaporation system shown in section 3.2.3 on page 13 is regulated from an external device, calibration is necessary. The voltage regulator was set up as illustrated in fig. A.1 on page 40. The voltage was increased from $0 - 140$V with increments of 20 lasting for 5 minutes for each level. The power (P) and intensity (A) values were monitored from the Co-Tech power meter. Both properties had minimum and maximum values, and were plotted in Excel. One would deduct that calibration is not needed for such an instrument, however, it is important to observe whether the regulator can provide sufficient power to the evaporation system. Moreover, a sensitivity test was performed on the regulator. The main purpose is to examine whether the volume change in the glass flask is approximately the same as the volume change through the upper flow meter after boiling time.

Additional procedures The previous paragraphs detail procedures performed before the experiment and these are conducted before the steps explained under this paragraph. These following steps should be done ideally the day before the main experiment, so that the temperature of the salt mixture in the setup is approximately room temperature.

(1) **Close the lower valve.** Make sure that the long arrow of the valve points towards the Arctic basin. Place a clamp right before the flow meter.

(2) **Fill the setup with salt mixture.** This is done at the Atlantic side with a 1000ml beaker up to the wireless temperature sensor (A2).

(3) **Remove air bubbles at the lower valve.** Unfasten the clamp first then open the valve.

(4) **Remove air bubbles through the replacement valve.**

   (a) Install a clamp on the capillary tube at the entry from the Atlantic basin to the evaporation system and close the replacement valve (90°).

   (b) Install clamps at the exit between the evaporation system and before replacement valve.

   (c) Remove the upper flow meter by installing clamps at the capillary tubes from the Arctic line and to the buffer system pictured in figure 3.5on page 17. Install the flow meter between the replacement valve and evaporation system, and remove the clamps.

   (d) Fill the glass flask pictured in figure 3.4on page 15 to 5cm above the entry from the Atlantic basin and open the replacement valve (180°).

   (e) Ensure that air bubbles are removed and close the replacement valve once the water level reaches the injection tube.

(5) **Fill up the setup.** Do so up to the mark at approximately 4m and remove the clamp situated in 4a. Remember to keep the salt mixture level in the setup the same along the way.

(6) **Fill up the buffer system with fresh water.** Figure 3.5on page 17 illustrates the system. Make sure to fill up above the marked 3.5L in container 1 and at the 3L mark in container 2. Start the buffer pump to remove air bubbles.

(7) **Determine flow rate at the replacement valve.** Recall 4c and connect the flow meter to a laptop to log the flow rate. Regulate the valve opening and stop at where the water level in the evaporation system is constant. Keep note of the flow rate in ml/min, install clamps as in 4b, remove the upper flow meter and reinstall the tubing.

(8) **Reinstall upper flow meter.** Connect the flow meter first to the Polar line then to the buffer system. Remove the clamps in 4c.

(9) **Install PASCO Interface and run PASCO Capstone.** Connect all sensors to PASCO Interface using figure 3.8on page 19 as guide. Remember to label them as shown in the figure. In PASCO Capstone, use 10Hz as a rate, therefore establishing that all record 10 measurements in a second.

(10) **Remove air bubbles in the PP3300 model VWR peristaltic pumps.** Alternate between starting and stopping to make remove air bubbles. Stop the process once the display values are constant and the pump drags less water from the Erlenmeyer flasks.

(11) **Connect two desktop displays together.** Do so by using VGA connector from desktop situated by the VWR pumps up to the desktop at the first floor. Install wireless mouse and keyboard by placing a Bluetooth chip in the lower desktop.

(12) **Connect power supply to the evaporation system.** Connect an extension cord to the 16A circuit as figure A.1on the following page illustrates. Insert an additional extension cord to the previous cord. The voltage regulator is then connected to the hotplate and power meter. Lastly, the power meter is connected to the second extension cord.

Experimental procedures

(1) **Start the water baths.** Check that the display illuminates the correct temperature for the respective basins.

(2) **Get all external devices ready for use.** This includes the laptop used to connect the upper flow meter, the wireless mouse and keyboard at the second floor.

(3) **Prepare PASCO Interface and Capstone.** Connect all the sensors and remember to calibrate the salinity sensors using the steps explained in (b) on page 37.

(4) **Start the VWR peristaltic pumps.** 139RPM and 150RPM for the Arctic and Atlantic basin respectively.

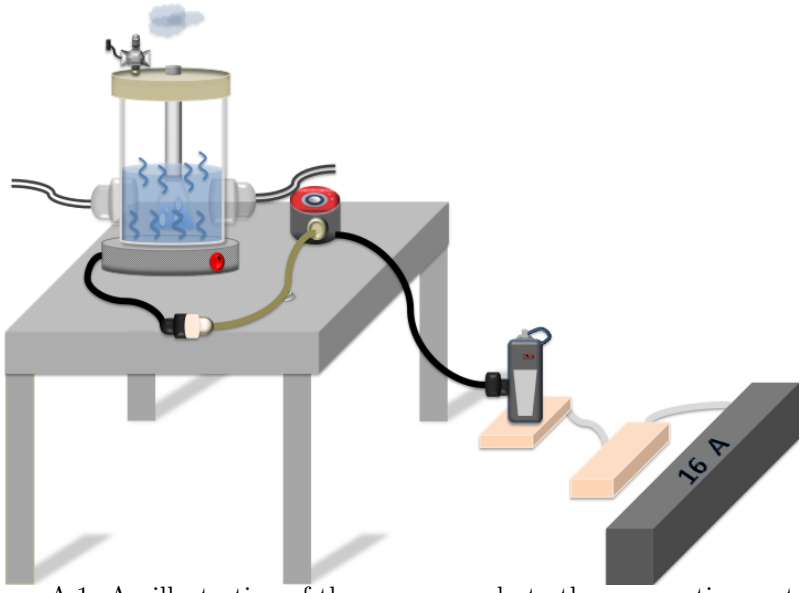

Figure A.1: An illustration of the power supply to the evaporation system.

(5) **Install plastic protractor at the replacement valve.** Repeat (4a), (4b) and (4c) on page 38. Take note of the flow meter readings as (7) on page 39 and use the protractor to determine at which angle the water level in the evaporation system is constant. Repeat (8) at page 39.

(6) **Start the buffer pump.** Use the following values 6.3V, 0.4A to initiate the pump. An indicator that the water level in the system is accurate is when excess water is flowing from container 1 to container 2 as pictured in figure 3.5on page 17.

(7) **Open the software USB RS485 Sensor View.** Make sure the upper and lower flow meter are connected to a laptop and desktop respectively. In the software:

(i) In the first window, choose "Liquid Flow Sensor" as a sensor product. Choose "RS485 Sensor Cable" as the COM Hardware. Press OK.

(ii) During the second window, determine the COM-port. An error will occur. Go through all port options until you access the third window "Liquid Flow Viewer".

(iii) Remember to select the right file. Use 100ms as a sampling time, a relative time information, linearized flow as the type of measurement and the resolution at 16 bit. All other setting are default, except for the average filter set at 80 for the lower flow meter. The upper flow meter is considered stable at 0.2ml/min.

(iv) Click "Run".

(8) **Start the experiment.** Remember to synchronize the clocks on the desktop displays. Start the evaporation system. Click "Start logging" in flow meter software and submerge the heat coil wires in their respective water baths.

(9) **Stop the experiment.** Close the replacement valve. Stop the evaporation system and the logging. Close the VWR pumps and repeat (4a) on page 38. Repeat (1), but do not close the lower valve, however close the upper valve. Repeat the beginning of (4c) on page 38. Stop the air injection process and the water baths.

(10) **Take water samples.** Do so for each basin and the glass flask.

(11) **Eject and cleanse.** Option the lower valve for opening, place a fairly large plastic container and unfasten the cap. Deposit of the mixture in a drain. Close the valve, use a tube to transfer freshwater into the setup and cleanse the setup $2-3$ times.

(12) **Store devices.** This includes the laptop, flow meters and other external equipment.

B Additional equations

B.1 1 box model

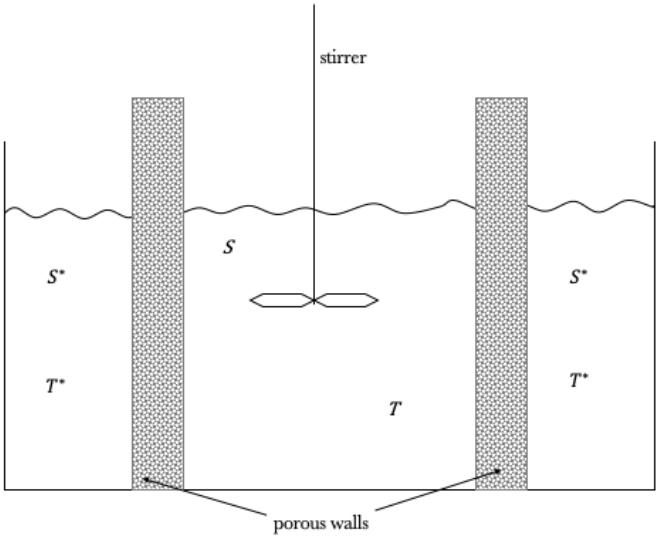

Figure B.1: Heat and salinity are exchanges between the compartments through the porous walls with constant temperature T* and salinity S*. (Walsh, 2019)

By deducting that temperature and salinity are dependant on time and not position, the equation below is given. (Walsh, 2019)

$$\frac{dT}{dt} = c(T^* - T) \qquad \frac{dS}{dt} = d(S^* - S) \tag{B.1.1}$$

The temperature transfer coefficient $c > 0$ and salinity transfer coefficient $d > 0$ are constants

with dimensions $[s^{-1}]$. In order to replace with physical parameters c, d, T^* and S^*, we *non-dimensionalize* them and obtain the following. (Walsh, 2019)

$$\frac{dx}{dt} = \frac{1}{S^*}\frac{dS}{dt} = \frac{1}{S^*}(d(S^* - S)) = d(1-x)$$
$$\frac{dy}{dt} = \frac{1}{T^*}\frac{dT}{dt} = \frac{1}{T^*}(c(T^* - T)) = c(1-y)$$

Remove d and c by setting $\tau = ct$ (dimensionless time) and $\delta = d/c$ (dimensionless ratio) thus obtaining the following. (Walsh, 2019)

$$\begin{aligned}
\frac{dx}{d(\tau/c)} &= \delta c(1-x) \\
c^2\frac{dx}{cd\tau - dc\tau} &= \delta c(1-x) \\
c^2\frac{dx}{cd\tau} &= \delta c(1-x) \\
c\frac{dx}{d\tau} &= \delta c(S^* - S) \\
\frac{dx}{d\tau} &= \delta(1-x)
\end{aligned} \tag{B.1.2}$$

$$\begin{aligned}
\frac{dy}{d(\tau/c)} &= c(1-y) \\
c^2\frac{dy}{cd\tau - dc\tau} &= c(1-y) \\
c^2\frac{dy}{cd\tau} &= c(1-y) \\
c\frac{dy}{d\tau} &= c(1-y) \\
\frac{dy}{d\tau} &= (1-y)
\end{aligned} \tag{B.1.3}$$

A simple equation B.1.4 for the density, where ρ (g/cm^3) is density, ρ_0 is the reference density (at $T = S = 0$), α $(^\circ\mathrm{C}^{-1})$ and β (psu^{-1}) are positive constants (Walsh, 2019). Setting $S = xS^*$ and $T = yT^*$, we get:

$$\rho = \rho_0(1 + T\alpha + S\beta) \tag{B.1.4}$$

$$\rho = \rho_0(1 - yT^*\alpha + xS^*\beta) = \rho_0(1 + T^*\alpha(-y + xR)) \tag{B.1.5}$$

where $R = \beta S^*/\alpha T^* > 0$ is a dimensionless constant. Stommel (1961) set $R = 2$ as the density at equilibrium point $(x, y) = (1, 1)$ is greater than at $(x, y) = (0, 0)$ if $R > 1$. Recalling B.1.5, we can obtain a dimensionless density anomaly σ:

$$\begin{aligned}
\rho &= \rho_0(1 + T^*\alpha(-y + xR)) \\
\rho &= \rho_0 + \rho_0 T^*\alpha(-y + xR) \\
\rho - \rho_0 &= \rho_0 T^*\alpha(-y + xR) \\
\frac{\rho - \rho_0}{\rho_0 T^*\alpha} &= -y + xR \\
\sigma &= \frac{1}{T^*\alpha}\left(\frac{\rho}{\rho_0} - 1\right) = -y + xR
\end{aligned} \tag{B.1.6}$$

B.2 1 box model with inflow and outflow

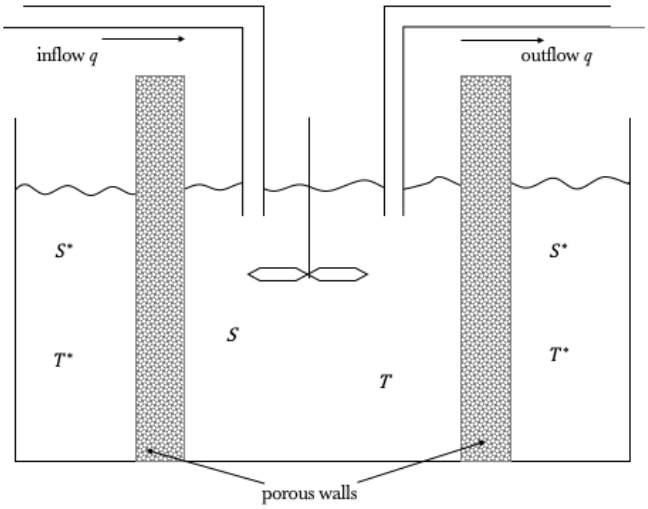

Figure B.2: Inflow and outflow is included with incoming water at a fixed temperature $T = T_{in}$ and salinity $S = S_{in}$. (Walsh, 2019)

Given that we now have an inflow and outflow, equation B.1.1 would look different in this case as given below. (Walsh, 2019)

$$\frac{dT}{dt} = c(T^* - T) + qT_{in} - qT \qquad \frac{dS}{dt} = d(S^* - S) + qS_{in} - qS \tag{B.2.1}$$

Using non-dimensionalizing by setting $u = T - T_{in}$ and $v = S - S_{in}$, where $u^* = T^* - T_{in}$ and $v^* = S^* - S_{in}$, and $x = v/v^*$, $y = u/u^*$, $\delta = d/c$ and $f = q/c$ (dimensionless flow), we obtain the following equations below. (Walsh, 2019)

$$\begin{aligned}
\frac{du}{dt} = \frac{dT}{dt} &= c(T^* - T) + qT_{in} - qT \\
&= c(T^* - u - T_{in}) + qT_{in} - q(u + T_{in}) \\
&= c(u^* - u) + qT_{in} - qu - qT_{in} \\
&= c(u^* - u) + qu
\end{aligned}$$

$$\begin{aligned}
\frac{dv}{dt} = \frac{dS}{dt} &= d(S^* - S) + qS_{in} - qS \\
&= d(v^* - v - S_{in}) + qS_{in} - q(v + S_{in}) \\
&= d(v^* - v) + qS_{in} - qv - qS_{in} \\
&= d(v^* - v) + qv
\end{aligned}$$

$$
\begin{aligned}
\frac{du}{dt} &= c(u^* - u) + qu \\
\frac{d(yu^*)}{d(\tau/c)} &= c(u^* - u) + qu \\
c^2 \frac{dyu^* + ydu^*}{d\tau c - \tau dc} &= c(u^* - u) + qu \\
u^* c^2 \frac{dy}{d\tau c} &= c(u^* - u) + qu \\
u^* \frac{dy}{d\tau} &= (u^* - u) + fu \\
\frac{dy}{d\tau} &= 1 - (1 + f)y
\end{aligned} \tag{B.2.2}
$$

$$
\begin{aligned}
\frac{dv}{dt} &= d(v^* - v) + qv \\
\frac{d(xv^*)}{d(\tau/c)} &= d(v^* - v) + qv \\
c^2 \frac{dxv^* + xdv^*}{d\tau c - \tau dc} &= d(v^* - v) + qv \\
v^* c^2 \frac{x}{d\tau c} &= d(v^* - v) + qv \\
v^* \frac{dx}{d\tau} &= \delta(v^* - v) + fv \\
\frac{dx}{d\tau} &= \delta - (\delta + f)x
\end{aligned} \tag{B.2.3}
$$

With the the equilibrium solution (at $dx/d\tau = dy/d\tau = 0$) below. (Walsh, 2019)

$$
(x^*, y^*) = \left(\frac{\delta}{\delta + f}, \frac{1}{1 + f} \right) \tag{B.2.4}
$$

Setting $\rho = \rho_0(1 - \alpha u + \beta v)$ where ρ_0 denote the density at entry when $(u, v) = (0, 0)$ at T_{in} and S_{in}, the density anomaly at equilibrium as shown below. (Walsh, 2019)

$$
\begin{aligned}
\sigma^* &= \frac{1}{u^* \alpha} \left(\frac{\rho}{\rho_0} - 1 \right) \\
&= -y^* + x^* R \\
&= -\frac{1}{1 + f} + \frac{R\sigma}{\sigma + f}
\end{aligned} \tag{B.2.5}
$$

C Additional figures

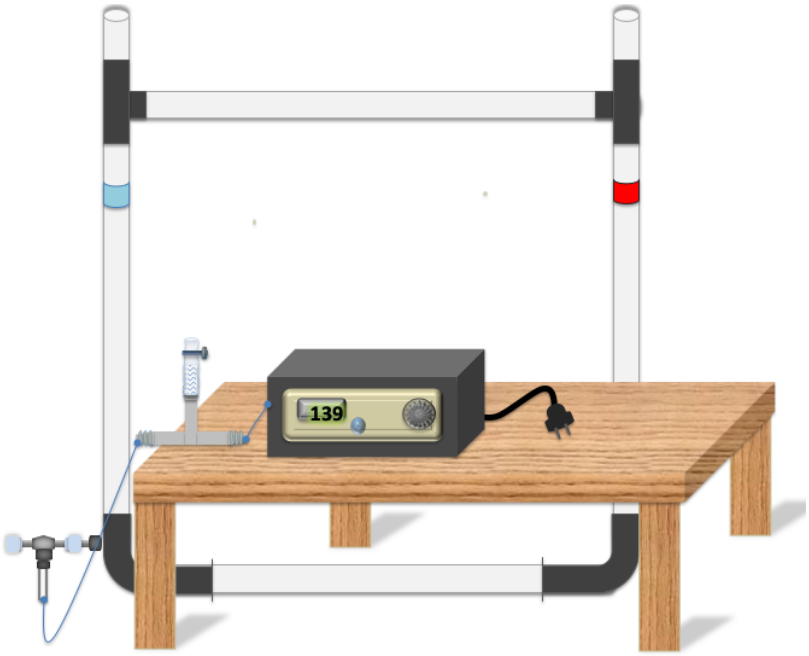

Figure C.1: The Erlenmeyer flasks shown in figure fig. 3.8 on page 19 are replaced with a three way passage connector, with a small capillary tube connected to the top passage with a clamp to ensure a constant pressure while pumping.

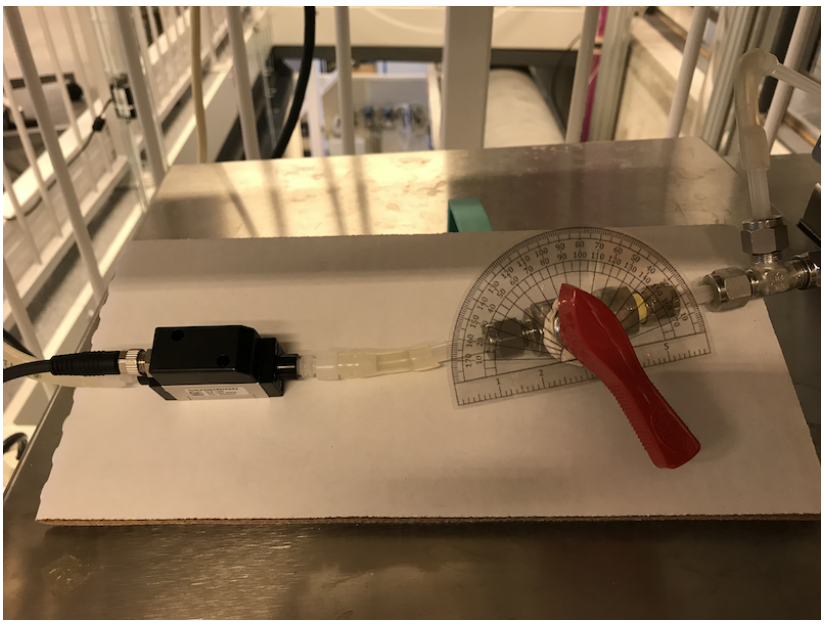

Figure C.2: The replacement valve installed by the evaporation system in fig. 3.4 on page 15 and the Atlantic basin water bath. The flow meter was used to ensure that the water level in the evaporation system was constant.

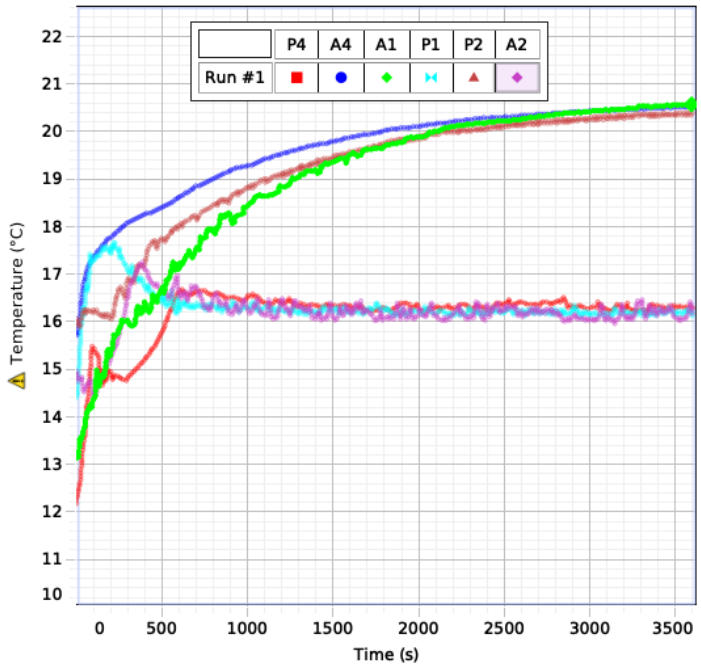

Figure C.3: First run before calibration. A lot of oscillations.

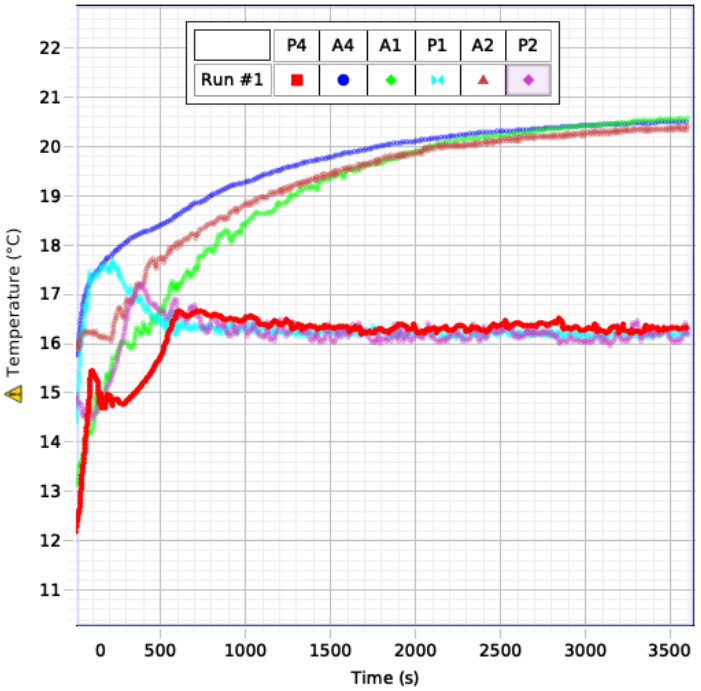

Figure C.4: Second run before calibration. No different from figure C.3.

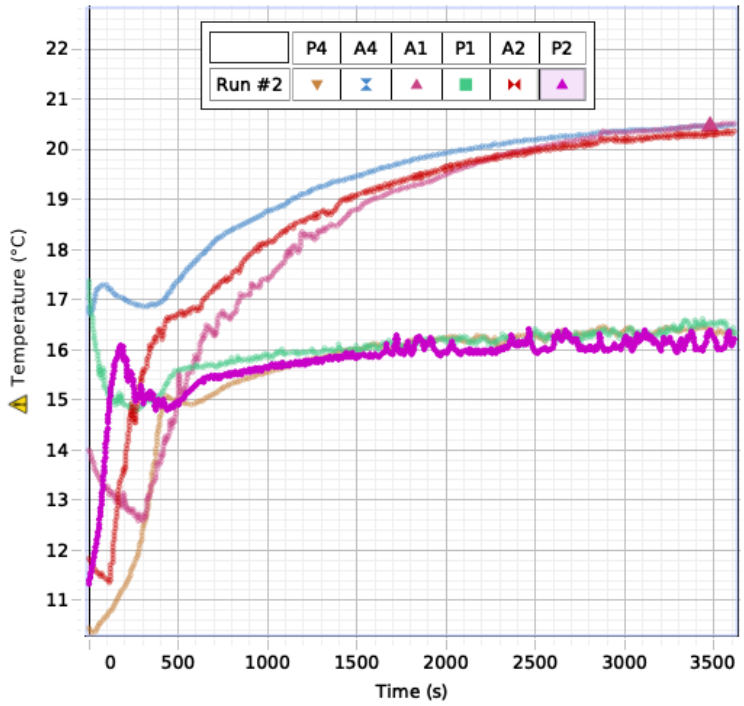

Figure C.5: Third run before calibration. Starting point for few sensors is lowered.

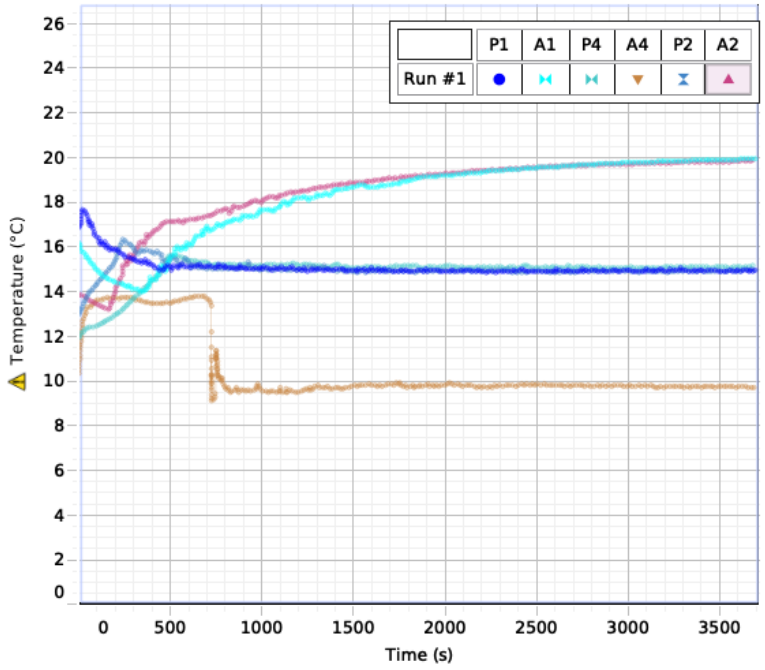

Figure C.6: Second run after calibration and lowered Arctic water bath temperature with defect A4 sensor.

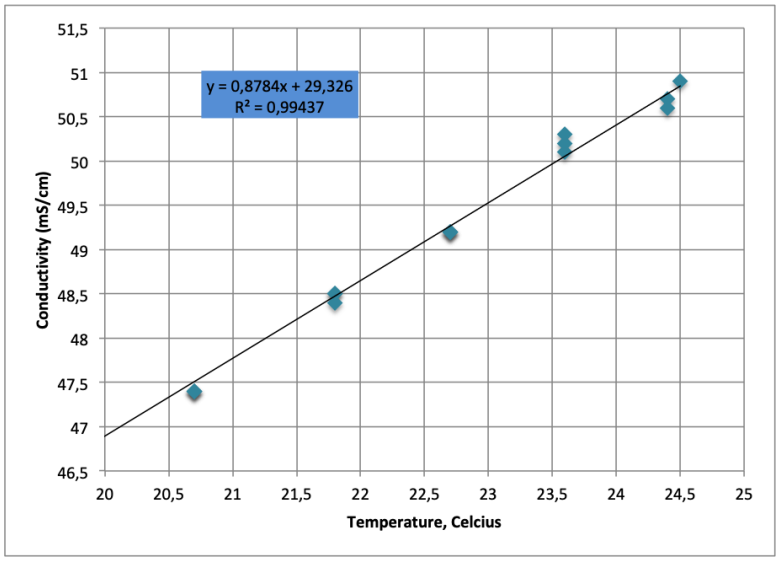

Figure C.7: Mettler Toledo values of the calibration solution before averaging with formula and R^2-number.

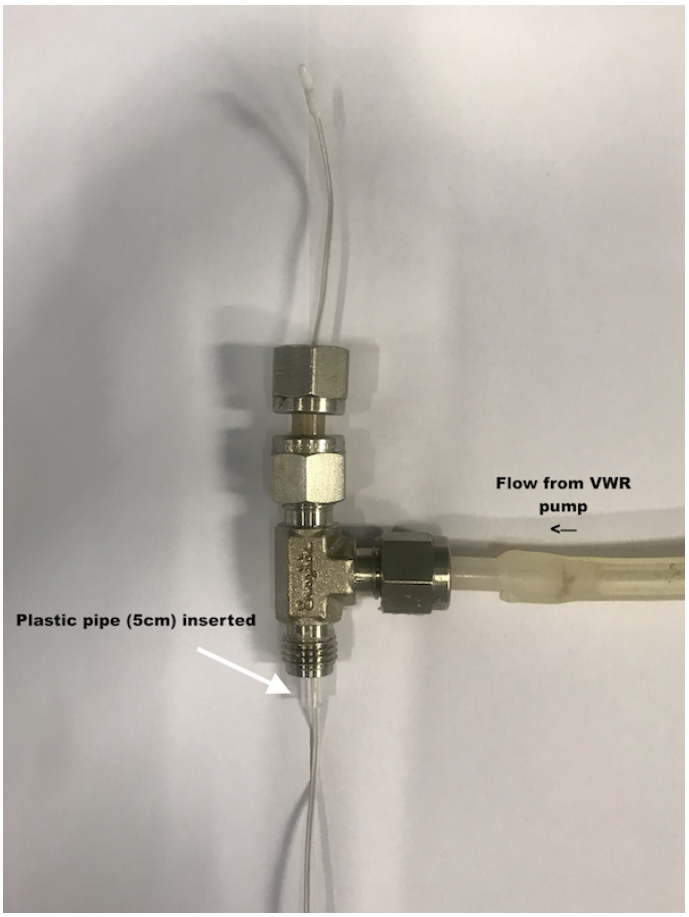

Figure C.8: Sensors $P4$ and $A4$ are both inserted with a plastic pipe.